

Progress in silica polypeptide composite colloidal hybrids: from silica cores to fuzzy shells

Cornelia Rosu · Sibel Selcuk · Erick Soto-Cantu ·
Paul S. Russo

Received: 3 November 2013 / Revised: 25 January 2014 / Accepted: 27 January 2014 / Published online: 11 March 2014
© Springer-Verlag Berlin Heidelberg 2014

Abstract Core–shell particles have attracted increased interest in the past two decades. The properties of these composite materials are a symbiosis between the core and shell features which neither can exhibit separately. Polypeptide composite particles (PCPs) are a newly expanding field of hybrid materials with potential future impact in a broad variety of applications. In this review, we present an overview about the progress made on designing PCPs. Past and present limitations in the fabrication of the cores and shells alone will be outlined. A special emphasis will be placed on the future challenges directed to design better materials by expanding the architectural repertoire which will benefit their functionality and their range of applications. The review also presents possible future trends and challenges in engineering polypeptide-based materials as platforms for targeted applications.

Keywords Stöber silica · Silica-coated magnetite · Silica-coated cobalt · Superparamagnetic particles · Fluorescent particles · Stimuli-responsive polypeptides · Polypeptide composite colloidal hybrids · Disease-inspired materials

Introduction

Colloids have been used for various purposes since the earliest records of civilization in technological processes such as making paper, cosmetics, and soaps. Over time, technical improvements allowed the design of well-defined materials. One of these materials is colloidal silica, or silica sol, which consists of stable dispersions or sols of discrete particles made of amorphous silica. Nature is abundant in silicon sources such as quartz. One key difference between colloidal silica and quartz sand, which have the same chemical formula (SiO_2), is the size. Typical silica grains are from 1 to 5 nm in size, but this is increased to the micrometer scale during the growth process. The other key difference is crystallinity. Colloidal silica is usually amorphous while quartz is crystalline. Silica has advantages over other inorganic materials; it is nontoxic, inexpensive and its relatively low refractive index proves convenient for many optical applications.

The range of silica applications is considerably expanded by adding dye labels and/or magnetic inclusions. For example, tagged colloidal particles can be used as tracers to understand diffusion in colloidal dispersions or in very viscous liquids, as shown by the Philipse group [1]. A magnetic inclusion inside the colloidal silica adds a degree of complexity that is especially appealing for biological applications [2]. Martel et al. reported the manipulation of colloidal magnetic beads at speeds on the order of $8 \mu\text{m s}^{-1}$ along preplanned paths by magnetotactic bacteria [3].

Core–shell particles having a well-defined solid core made of silica and a polymer coating have enhanced colloidal stability and robustness, as reviewed by Zou et al. [4]. In the past, few composite materials have been made featuring a homopolypeptide anchored to a silicon surface. For a convenient literature entry, see a few representative references [5–8]. The advantage of these composite particles is that, in the same material, the chemical versatility of the polypeptide shell is

C. Rosu · S. Selcuk · E. Soto-Cantu · P. S. Russo (✉)
Department of Chemistry and Macromolecular Studies Group,
Louisiana State University, Baton Rouge, LA 70803, USA
e-mail: paul.russo@mse.gatech.edu

Present Address:
P. S. Russo
School of Materials Science and Engineering, Georgia Institute of
Technology, Atlanta, GA 30332, USA

combined with optical and physical properties of the core [9]. Depending on their side chain substituent, polypeptides can deliver a variety of versatile properties such as chirality, ability to form liquid crystals, secondary structural changes as a response to external stimuli, etc. No less important than self-assembly in spherical and cylindrical micelles or vesicles is the ability of polypeptides to form liquid crystalline phases [10–14]. Polypeptides undergo conformational transitions induced by the temperature, solvent, pH, and surfactants. Doty and Yang [15], Blout and Lenormant [16], and Applequist [17] conducted pioneering studies on poly(γ -benzyl-L-glutamate) (PBLG) helix-coil transition. Other researchers have also investigated the nature of PBLG secondary transitions [18–21]. Polytyrosine undergoes a helix-coil transition in mixtures of dimethylsulfoxide (DMSO) and dichloroacetic acid [22]. Poly(N^{ϵ} -carbobenzyloxy-L-lysine) (PCBL) has a reverse transition from helix to coil in m-cresol as a function of temperature [23]. Poly(β -benzyl-L-aspartate) is another polypeptide known to change its conformation in m-cresol [24]. Deprotection of side chains of the PBLG, PCBL, etc., enables the pH-dependent conformational transitions [25]. Helix-to-helix [26] or helix-to-sheet [27] changes were also reported. When one tethers these polypeptides on a spherical bead, the resulting hybrid is similar in overall structure with protein-caged materials like viruses. Perhaps the most interesting aspect of research in this field would be to elucidate the powerful mechanism viruses have to kill a living body and take that power and use it for positive purposes. Polypeptide composite particles (PCPs) can serve as platforms for these studies.

The review proceeds as does the synthesis of the particles—from core towards shell. Readers familiar with the individual parts of the particles—silica cores, superparamagnetic inclusions, and polypeptides—are invited to jump ahead to “[Routes to silica-polypeptide hybrids](#)” section, which deals with the hybrid composite particles as a whole.

Colloidal silica-based cores

Historical perspective on colloidal silica sols

The facile preparation of silica particles makes them the most popular choice for basic research. In this respect, researchers have to be able to tune the quality of these products by controlling the size and size distribution of resulting silica. Concentrated silica sols that were stable against gelation and precipitation were reported [28] in the 1940s. Vail in 1925 and Treadwell and Wieland in 1930 prepared sols that contained more than 10 % silica particles but were not stable to the gelling effect. Ammonia-stabilized sols were reported by Griessbach in 1933. Later in 1941, Bird et al. prepared 5–10-nm-sized particles by removing alkali from dilute sodium silicate using hydrogen ion-exchange resin, followed by

stabilization with dilute alkali and concentration of the solution. White et al. used the process of peptizing the gel to a sol by dispersion in a basic solution and heating. Better control on the size and the uniformity was achieved by Bechtold et al. in 1951. Bechtold’s method was improved by Rule et al. by optimizing the concentrations of alkali used for stabilization. All the above reports on silica suspensions were summarized in the Iler book [28].

One-time addition of silicon alkoxide

In 1956, Kolbe [29] reported the first narrow-size-distribution silica particles made by hydrolysis and condensation of a silicon alkoxide, tetraethyl orthosilicate (TEOS), in a mixture of alcohol, water, and ammonia. The first systematic study and probably the most cited work on narrowly distributed colloidal silica was performed by Stöber et al. in 1968 [30]. Particle diameters ranged from several hundred nanometers to 2 μm . The synthetic procedure used ammonia-catalyzed hydrolysis of silicon alkoxides of different chain lengths and subsequent condensation of the silicic acid in the alcoholic solutions. The key to the Stöber procedure, illustrated in Scheme 1, is the use of highly pure tetra-alkyl silicates obtained by redistillation. Since the Stöber report, the most popular silanization agent has been TEOS [31].

Silane-based polymers condense in a compact state, leaving –OH groups on the exterior. The degree of this compact state depends on the reaction conditions, as shown by Van Helden et al. [32]. Even though the hydrolysis–condensation reactions can occur over a wide range of pH, only between 7 and 10 and in the absence of the salts are all the condensed species ionized and therefore mutually repulsive.

Because TEOS does not mix with water, a small alcohol (MeOH, EtOH) is added. Bogush et al. expanded the range of the reagent concentration and the reaction temperature and obtained 17 % yield with narrow distribution and good control over size [33]. They proposed an expression to predict the diameter of the particle as a function of reagent concentrations:

$$d = A[\text{H}_2\text{O}]^2 \times \exp(-B[\text{H}_2\text{O}]^{1/2}) \quad (1)$$

where

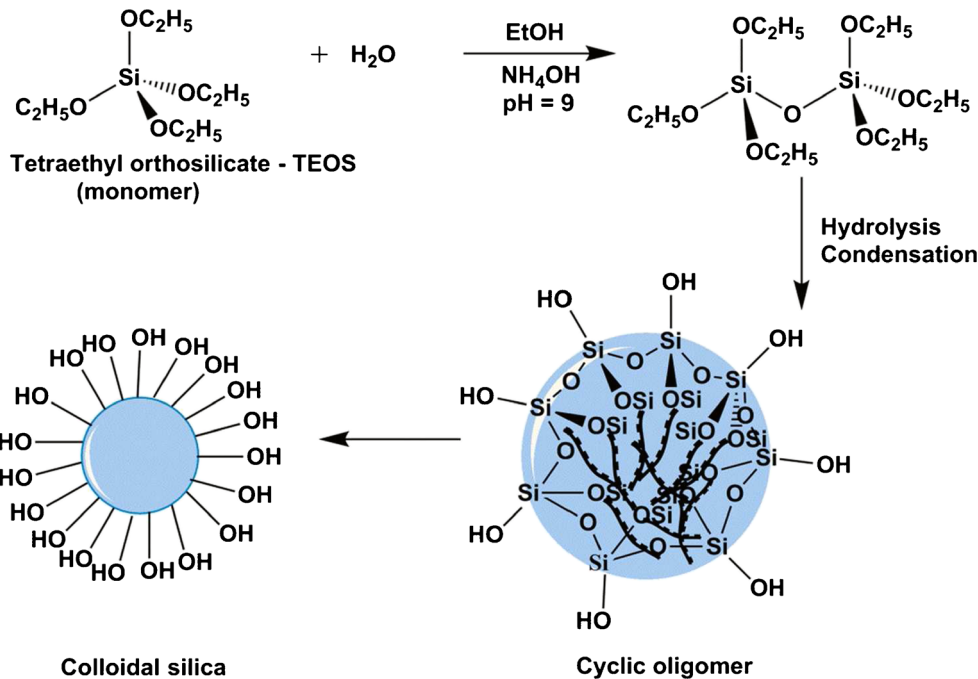
$$A = [\text{TEOS}]^{1/2} \times (82 + 151[\text{NH}_3] + 1,200[\text{NH}_3]^2 - 366[\text{NH}_3]^3)$$

and

$$B = 1.05 + 0.523[\text{NH}_3] - 0.128[\text{NH}_3]^2$$

In this equation, d is the average diameter in nanometers and reagent concentrations are expressed in mole per liter.

Scheme 1 Schematic illustration of the Stöber method



Equation 1 is the corrected version proposed by Bogush. The initial formulation had a minus sign in front of the ammonia concentration ($-151[\text{NH}_3]$).

The controlled aggregation model proposed by Bogush and collaborators treated the nucleation and growth of silica as an aggregation of nanometer-scale silica grains [34]. Matsoukas and Gulari explained the nucleation through the monomer addition model: the nucleation arises as a result of the hydrolysis between two monomers followed by the growth through molecular addition [35]. These two models are akin to condensation versus addition polymerization. Many studies were developed, as summarized in Brinker and Scherer's book [31].

All the Stöber-like processes yield a broad range of sizes with narrow particle distribution but the drawback is the low solid weight fraction of the particles. An increase in the concentration of the TEOS results in heterodisperse sols because of the second nucleation. In order to attain narrow distributions, larger particles, and higher solid yield, Bogush, Tracy, and Zukoski (BTZ) pioneered the seed method, sometimes called the regrowth method [33].

Seed method—a route to particles with narrow distributions

In a typical seed method experiment, a suspension of the silica particles is prepared and further amounts of the TEOS are added to achieve the desired size.

Bogush et al. used seeds of 170 nm in diameter, fabricated from distilled TEOS, and added sequential portions of TEOS equal to the volume used for seeds. After ten additions at 8 h intervals, the stable suspensions were analyzed and the silica colloids were found to keep their spherical shape and narrow

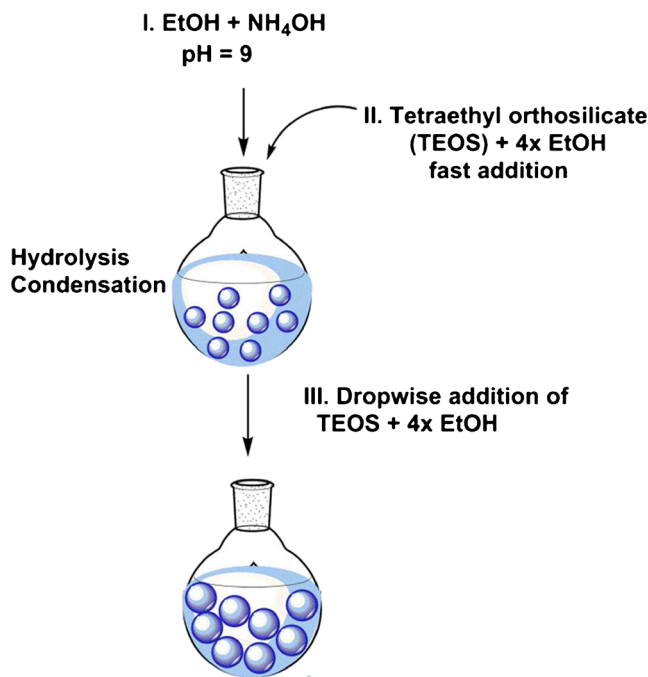
distributions, while size increased significantly. The mass fraction of solids increased to an upper limit of 24 %. They correlated the size of the final particle with the volume of the TEOS used:

$$d = d_0 \left(\frac{V}{V_0} \right)^{1/3} \quad (2)$$

where d is the final average diameter, d_0 is the average seed diameter, V_0 is the volume of TEOS used for the seed production, and V is the total volume of TEOS added.

It was also found that using TEOS as received (no distillation) in the subsequent growth steps did not impact the particle shape and distribution.

Extra purification of silicon precursors increases the cost of production. Consequently, the combination of the original Stöber and Bogush's seed methods was streamlined to use technical-grade TEOS. Zhang et al. [36] obtained silica colloidal particles with uniform size, shape, and composition following the BTZ formulation [33], as depicted in Scheme 2. Zhang's unique contribution was to dilute TEOS four times with ethanol rather than to distill it for seed production and further regrowth. In the subsequent regrowth steps, the diluted TEOS was continuously added dropwise. This approach was inspired by previous reports which showed that undesired sizes and shapes (e.g., "peanut") cannot be avoided when technical-grade TEOS is used without dilution. The use of TEOS with no dilution over 8 h addition intervals led to a long period of growth. Dilution of TEOS with ethanol was found to be an effective way to shorten the nucleation and the growth



Scheme 2 Schematic illustration of the seed method

times thus suppressing undesired shapes and sizes. The dilution improves the diffusion rate of the reagents and the nascent nuclei have a greater probability to grow without secondary nucleation. It also depresses the adhesion or aggregation of the particles. The method developed by Zhang et al. proved efficient for preparing silica in the 150 to 1,200 nm size (diameter) range with a percentage standard deviation from ± 5 to ± 1 %, respectively.

Recently, Watanabe et al. prepared particles with a narrow size distribution by the seed method using L-arginine for nucleation [37]. Seeds with a narrow size distribution were prepared by emulsion in a mixture containing L-arginine and TEOS. Various particle sizes were obtained by addition of TEOS to the original seed sol and additional small amounts of L-arginine. This method underlines the importance of the seed quality. Spherical and narrow-distribution seeds lead to even better colloidal materials in terms of size dispersity after sequential growth by the TEOS addition. Other seeded methods to make silica have been reported [38, 39]. Balamurugan and Saravanan even used actual plant seeds (from *Sorghum vulgare*, an agricultural waste) to seed silica growth [40].

Magnetic cores

Magnetite

Ferrites are ceramic-like ferromagnetic materials, mainly composed of $\alpha\text{-Fe}_2\text{O}_3$ [41]. One of the most important

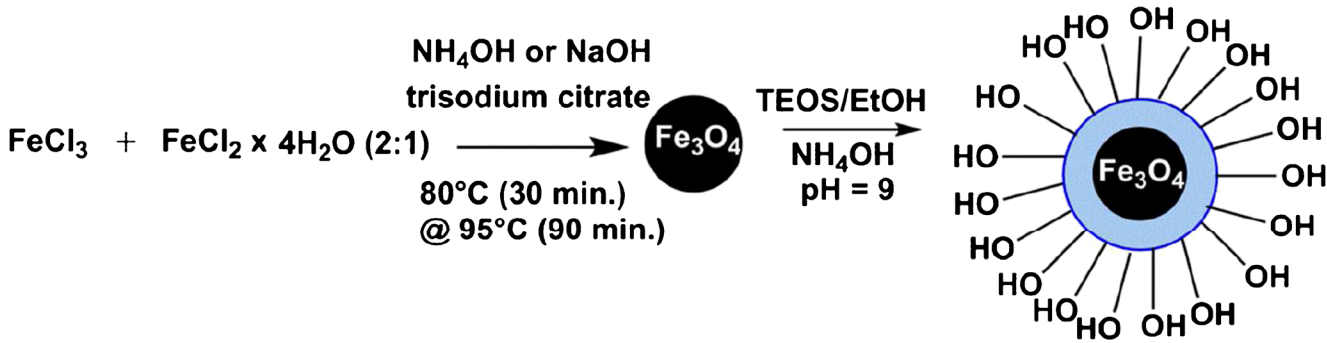
magnetic materials is magnetite, Fe_3O_4 , which comes from the ferrite family. Its discovery dates back in time to the legend of the shepherd Magnés. While herding sheep on Mount Ida, his metal-tipped walking stick was attracted to the ground, as were his shoes due to the nails used in their soles. When he dug in the ground to find what was pinning his boots thereto, he found stones that today are referred to as lodestones containing magnetite. The actual discovery of lodestones can be attributed to either the Greeks or Chinese. Magnetite is also used by magnetotactic bacteria, *Aquaspirillum magnetotacticum*, microorganisms found in fresh water. They contain fine Fe_3O_4 particles and are capable of orienting along the Earth's magnetic field which enables them to swim in a given direction. In the laboratory, Smiltens et al. prepared, for the first time, large crystals of magnetite as described in Rado and Suhl's book [42]. Over the years, several methods were developed to synthesize functional magnetic nanoparticles with controllable size and shape driven from their broad technological applications.

Coprecipitation method and silica coating

The preparation of ferrofluids containing magnetite is usually performed in both acidic and basic solution by mixing the appropriate amounts of an iron(II) and iron(III) salts. Magnetite, Fe_3O_4 , is the resulting black precipitate from a mixture of two oxides (Fe(II) and Fe(III)), $\text{FeO}\cdot\text{Fe}_2\text{O}_3$. The earliest coprecipitation preparation of Fe_3O_4 was accomplished by the Bureau of Mines [43]. Later, this technique was modified by Massart. This is one of the most cited reports on ferrofluid production [44]. In order to prevent the oxidation of the magnetite particles, Massart stabilized the dispersion with different peptizing agents in both acidic and basic media. Philipse et al. prepared silica-coated magnetite [45] and stabilized the magnetic nuggets with oleic acid prior to silica coating [46]. Coating magnetic particles with an inorganic matrix proved to be an efficient route to produce magnetic colloids. The iron surface has a high affinity toward silica. A silica shell not only prevents the magnetic particles from aggregation in different pH ranges but also provides a surface which can be further modified with various functionalities (Scheme 3).

Coprecipitation, also called the sol-gel method, has been adopted more widely because the yield of the silica-coated magnetite particles is high, even when the production of a uniform particle with a single magnetic inclusion is not well-controlled. In this regard, other reports tried to optimize the reaction conditions [47–52]. Advantages of the sol-gel approach over other methods are low cost, relatively mild reaction conditions, and absence of surfactants.

Systematic studies should regard all parameters involved in the synthesis of the magnetic particles, especially when the final particle is desired to have superparamagnetic properties.



Scheme 3 Schematic route for preparation of the silica-coated magnetite particles by coprecipitation method

This requires nanometer-sized grains (typically <15 nm in diameter). In this respect, Iida et al. found that varying the hydrolysis conditions by increasing or decreasing the reagents concentration, especially the ratio of the ferrous to ferric ions, led to larger Fe₃O₄ particles [53]. The magnetic properties could be controlled to some extent. When only ferrous sulfates or chloride salts were used in the preparation, the saturation magnetizations were 86.6 and 81.0 emu g⁻¹, respectively (in this article all magnetization values are reported as per gram of metal, usually iron or cobalt). A significant drop in the saturation magnetization when compared with the bulk magnetite, ~91 emu g⁻¹, was noted for samples prepared from both ferric and ferrous sulfates of chlorides, 46.7 and 55.4 emu g⁻¹, respectively. The trend was attributed to the oxidation of the ferric ion during the preparation, leading to a ferrimagnetic material. Other reports obtained the same values. They can be found in recently published reviews [54, 55]. Precipitation with a basic solution at temperatures below 60 °C led to the preferential formation of the maghemite, while temperature over 80 °C yielded magnetite [56]. Higher saturation magnetization, better crystallinity, and smaller particle size were achieved by using ammonium hydroxide solution instead of sodium hydroxide [57]. Also, pouring the alkali solution as quickly as possible into magnetite forming mixture under vigorous stirring resulted in a black coloration but the size dispersity of the magnetic particles was broad. A slow pouring favors less nucleation and the crystalline grains grow all at the same time [58]. The nuclei number remains constant and the added monomer molecules condense on the existing grains. The coprecipitation method may remind the reader of living addition polymerization, in which the absence of chain termination and chain transfer reactions, and a higher rate of initiation than propagation ensure the growth of the polymer chains at a constant rate. Their lengths are similar and the polydispersity index low. A fast addition of alkali solution would favor the formation of a high amount of nuclei, unable to grow as uniform crystallites. The formation of particles with a narrow size distribution relates to the ability of nascent nuclei to quickly adhere to each other.

Oxygen removal is essential to obtain pure magnetite particles. Unwanted oxidation is prevented by the presence of an inert atmosphere (e.g., argon or nitrogen bubbling). This approach not only prevents oxidation but enables a decrease in the particle size [57, 59]. Liu et al. demonstrated that when the deionized water was not degassed and the synthesis proceeded under ambient conditions without N₂ protection, a reddish-brown colloid was obtained, indicating the presence of other iron oxide phases as a consequence of Fe₃O₄ oxidation [58]. These phases impacted the magnetic properties of the desired magnetite by lowering the saturation magnetization or even arresting the superparamagnetic behavior. Small, superparamagnetic magnetite particles were prepared using coprecipitation by other research groups in various sizes: 6–7 nm diameter with 2 nm silica shell, 9.2, ~10, 10.4 and 12.3, 6 and 12, and 10 and 40 nm. The reports attest to the broad range of particle sizes described in several recent reviews [54, 55, 60].

Emulsion method

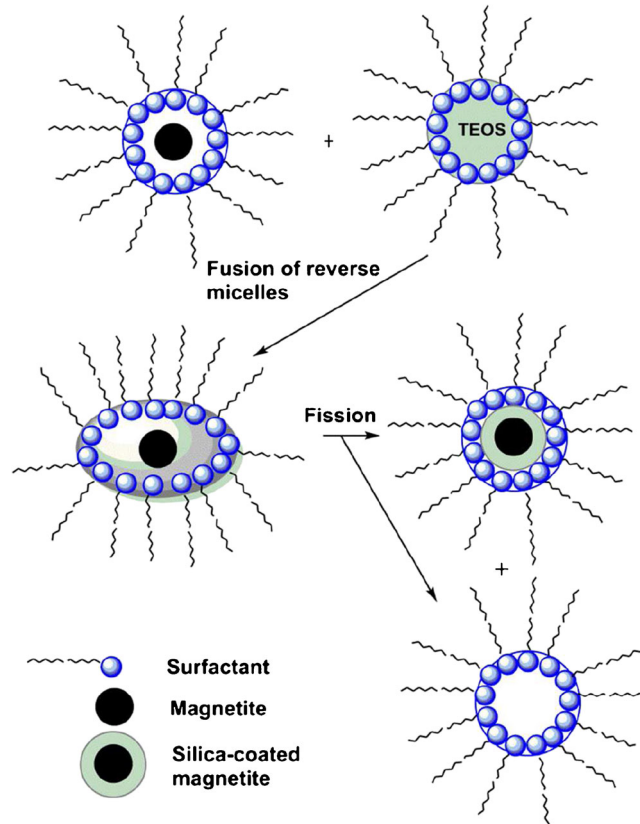
Preparation of colloids in emulsions has been regarded as an effective method to either produce narrow-size-distribution silica particles or encapsulate magnetic inclusions into silica or to produce a polymer shell. This paragraph will describe the fabrication of both silica and magnetite silica-coated particles. Emulsion is a general term to define micro- and macro-emulsions, reverse micelle, or inverse microemulsion. The difference is made by the interplay between the components of the water-in-oil emulsion. An amphiphilic surfactant is added in an attempt to lower the interfacial tension between water and oil. Droplet uniformity is an important determinant of quality of the final product. Inside the droplets, particle formation is a combination of nucleation, growth, coagulation, and flocculation, in some instances. The major advantage of the emulsion is the uniformity of the resulting particles. Reverse micelle is the most successful procedure used in the synthesis of colloidal particles with narrow distribution because the nucleation occurs simultaneously at a large scale

within the aqueous phase and it is separated by the growth due to the intermicellar interactions. The reverse micelle phase consists of surfactant-encapsulated water droplets, the aqueous pool physically separated by the oily phase. The challenge is in controlling the size of the pool droplets to obtain fine and narrow-distribution particles, as reviewed elsewhere [61]. The reverse micelle method has yielded, over the years, a broad spectrum of silica-based materials and it is reflected in Scheme 4 by an example of the silica coating of metal particles (e.g., magnetite).

The optimum condition found for the preparation of such products seems to point to a gradual increase of pH up to 11–12 after immersing the silica precursor, usually TEOS, in the water–ethanol phase. The condensation of TEOS must be catalyzed by a base or an acid. Ammonia is the most commonly used catalyst because it was noticed to yield good spherical morphologies of the particulates. The optimal temperature should be kept below 25 °C because of the possible thermally induced phase inversions. The reaction time has been reported from few hours up to 48 h for a complete reaction. The control over the size of the silica-based particle is obtained by tuning the TEOS/water/surfactant ratio.

The formation of the silica particle or the silica coatings by the reverse micellar system can be explained by a series of steps. Contradictory opinions have been formulated to explain the microemulsion mechanism; the most agreed-upon path for a mono-emulsion involves the association of TEOS molecules within the micelles, as the first step, after its addition into the emulsion phase. The catalyst then enables the hydrolysis of TEOS with the formation of the monomers. Nucleation occurs by condensation of monomers via inter- and intra-micellar exchange. Further nuclei growth is favored by addition of TEOS or by aggregation. A review [55] and a book chapter [62] list materials such as ferrofluids and metal, mixed-metal, and metal-oxide particles that have been prepared by the emulsion method.

Now let us take a look back over the microemulsion method and underline what might be considered as the future trends. Even though the micelle itself is considered a nanoreactor, the main drawback is the still-poor control over the reactions and the reaction conditions that govern the formation of a high-quality product. Spherical particles with a narrow size distribution were obtained but the method is still shadowed by the low yields of the final material. Yet, a combination with other synthesis techniques (e.g., sol–gel [63], hydrothermal/solvothermal [64]) can have various advantages: the fine and the tunable nucleus size obtained in the reverse micelle and the growth controlled by the stoichiometry through the sol–gel method. Combined techniques opened the door to more complex products. The layer-by-layer deposition of the oppositely charged electrolytes onto the particle surface [65], metal-doped carbon nanotubes [66], or polymer encapsulated nanoparticles [67] has been produced in the reverse



Scheme 4 Schematic illustration of the silica coating of metal particles using the reverse micelle

micellar systems. One intensively explored trend is the assembly in 3D supramolecular lattices, as reflected in a series of papers by Pileni and collaborators (most recently, a review [68]). Driven by external fields (e.g., magnetic or electric), self-assembled crystalline structures are considered a future challenge. The new combination of different surfactants may give rise to better control over the morphology and useful properties of the desired materials. Before ending this section, several reviews dedicated to this subject must be mentioned [55, 69, 70].

Cobalt

Instead of particles containing metal oxides, sometimes with difficult-to-reproduce mixed oxidation states, reduced metals such as Fe, Co, Ni, and their alloys can be used. In particular, cobalt attracted interest in the field of superparamagnetic materials because of its high saturation magnetization. The use of pure metals has difficulties arising from their instability toward oxidation in air. Once the particle size decreases, especially close to superparamagnetic limit (~10–15 nm), oxidation becomes easier. Thus, the preparatory approaches require ways to improve the chemical stability of the particles. Cobalt metal, which is highly sensitive to air, has two crystal

structures, face-centered cubic (fcc) and close-packed hexagonal (hcp). These structures coexist at room temperature, but at elevated temperature (450 °C), fcc is thermodynamically favored [71]. Consequently, the magnetic properties of cobalt greatly depend on the crystal nature and the temperature [72].

The era of cobalt particles began with a report by Hess et al. in 1966. They thermally decomposed dicobalt octacarbonyl in solutions of different polymers [73]. A cobalt organometallic precursor has been used by Ould-Ely et al. to prepare cobalt particles, which were coated with polyvinylpyrrolidone [74]. Coating procedures also included noble metals, used as insulating shells through the microemulsion method or other chemical approaches such as redox transmetallation [75]. Thus, Sobal et al. reported stable Ag-Co nanoparticles with cobalt as the shell [76]. Nikitenko et al. used a sonochemical procedure to obtain air-stable Co colloids [77]. The explanation behind the stability of the nanoparticles was the formation of a carbon shell on the particle surface. The pyrolysis of metal carbonyls was applied to produce Co, Fe, Ni, and other magnetic materials. The solution phase metal salt reduction was involved in the preparation of the Co, CoO, and FePt particles. The challenge in the above-mentioned reports was the control over stability and size. Particles were rather polydisperse and not very uniform.

The deposition of silica shells on the metal magnetic particles as a stabilizer was used in several reports [55]. The facile modification of the surface, the excellent stability of the aqueous solutions, and the good control on the interparticle interaction make silica one of the best candidates for coating metal nanoparticles. The complications in silica attachment arise due to the lack of functional groups, especially –OH, on the metal surface. Therefore, it is necessary to use a primer to enable silica deposition. For example, in 1996, Liz-Marzan et al. coated gold colloids with silica in a three-step deposition process [78]. First, citric acid was used as stabilizer that was then replaced with amino silane groups. Finally, silica was attached to the surface of the particles through the Stöber method. A better control over the size and the colloid stability, following the Liz-Marzan et al. procedure, was reported by Kobayashi et al. in 2003 [79]. They used a one-pot reaction, as shown in Scheme 5, to prepare silica-coated cobalt particles with different Co core size and silica shell thickness.

The authors demonstrated that sequential addition of the silica precursor, TEOS, improved the particle uniformity and the sphericity without altering the magnetic properties. Two crystal structures, fcc and hcp, of silica-coated cobalt particles were identified after annealing at different temperature (200–700 °C). After annealing at high temperature, these particles showed high magnetization saturation in the range of 120–180 emu(g cobalt)⁻¹. The methods to obtain silica-coated colloidal particles were reviewed by Guerrero-Martinez et al [80].

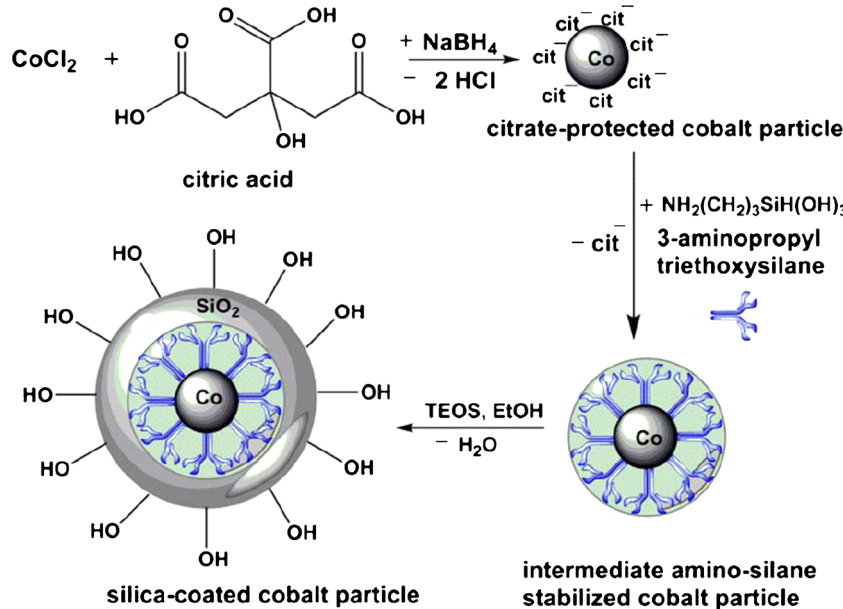
Solvothermal/thermal decomposition routes to iron and cobalt oxides

High-temperature methods can lead to magnetic materials with narrow size distributions, with benefits to applications requiring superparamagnetism. Metal oxides and alloys obtained through these methods showed high saturation magnetization [81]. Protection by using silica as primer can be achieved by the sol–gel approach. Let us have a glimpse over the high-temperature routes to metal oxide particles by using iron and iron precursors as an example. The thermal decomposition of organometallic precursors such as $\text{Fe}(\text{acac})_3$ ($\text{acac}=\text{acetylacetone}$) and $\text{Fe}(\text{CO})_5$ (carbonyls), assisted by organic solvents and surfactants is a reliable way to paucidisperse nanocrystallites ranging in diameter from 3 to 15 nm. The surfactants (ligand) are, in general, long-chain amines, fatty acids, or both. They have a dual role: to mediate the growth during reaction and to prevent particle aggregation. A satisfactory stabilization requires ligands at least six carbon atoms long [82]. A zerovalent metal precursor leads to the formation of a metal grain or cluster that can be subjected further to oxidation and give high-quality iron oxide particles. Cationic metal sources directly yield iron oxides. Control over the size distribution and morphology is achieved by optimizing the ratios of the starting materials (iron precursor, solvents, and surfactants). In addition, temperature and time complete the map of decisive factors in controlling the size and the dispersity.

Kwon et al. prepared iron oxide particles by thermal decomposition of the iron oleate complex in their effort to elucidate the kinetics [83]. The mechanism of the decomposition had been shown to evolve through intermediate species acting as monomers for iron oxide monocrystals, as shown in Scheme 6. The sudden increase in the concentration of the nanocrystals (burst crystallization) as evidenced by TEM was followed by a rapid decrease in size distribution (size focusing). Once the reaction time increased, the iron cluster grew unevenly.

The control over the ratio of surfactant to FeO(OH) led to a broad distribution of the sizes ranging from 8 to 55 nm, some with a high magnetization moment [84, 85]. Even though the thermal decomposition process yields particles with a narrow distribution, it is not environmentally friendly or economical. For example, the $\text{Fe}(\text{CO})_5$ precursor is highly toxic and ligands such as 1-octadecene and oleylamine are expensive [86]. Zhang et al. developed a green thermal chemistry using ethanol as solvent and 1,2-dodecanediol as ligand. The reaction mixture was held at 150 °C in an autoclave for 24 h. The iron clusters were comprised of 5 nm magnetite crystals [87]. Ultrafine magnetite powders are prepared by the hydrothermal method, also called the solvothermal method. The aqueous media is the major advantage of this reaction but high pressure (greater than 2,000 psi), high temperature (higher than

Scheme 5 Schematic of the surface reactions involved in the formation of silica-protected cobalt particles

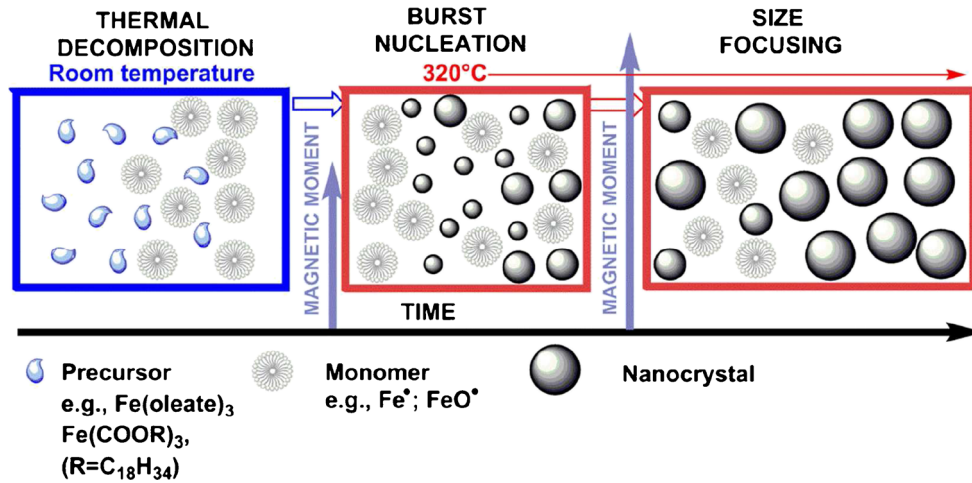


200 °C), and a good sealing are required once the mixture is placed into autoclave. The concentration of the iron source used in preparation can tune the size of the magnetic crystal and the nanocluster [88]. The continuous hydrothermal process is a simple route to metal oxide particles of the specific size and morphology. Although this route is environmentally friendly and can be scaled up easily, the mechanism of particle formation has not been yet determined. Investigations on factors that influence the evolution of the hydrothermal process were performed by Xu and Teja [89]. Particle size distribution and aggregation seemed to increase with increased concentration of polyvinyl alcohol, temperature, and time. Cobalt oxide cores can be produced from a precursor such as cobalt octacarbonyl, $\text{Co}(\text{CO})_8$, following the same

methodology as for magnetite obtained from $\text{Fe}(\text{CO})_5$ [90, 91]. Metal acetylacetones are other sources to fabricate mixtures of iron and cobalt oxides by hydrothermal methods as a future approach to particles with improved properties. They are less toxic for the living bodies and coating with silica broadens their spectrum of applications [92].

The drawback of the conventional hydrothermal method is the slow kinetics at any specific temperature. In an effort to speed the crystallization kinetics, Komarneni and Katsuki introduced a new approach termed microwave-solvothermal method [93]. The shorter time and thermal conditions allowed the production of particles in a 2- to 60-nm size range with good control over colloid dispersity. Balasubramanian et al.

Scheme 6 Schematic representation of the size, morphology, and magnetic properties as a function of the reaction temperature and reaction time for magnetite synthesized by thermal decomposition methods. Adapted from reference [83]



used DC thermal arc-plasma to prepare Fe_3O_4 powders having a high magnetization saturation, 88 emu g^{-1} [94].

Dye labeling

Labeling of the colloidal silica with fluorophores leads to materials with a broad spectrum of applications [95]. Various labeling agents can be incorporated into nanoparticles to yield fluorescent probes [95]. Dye-labeled nanoparticles, semiconductor quantum dots (Q-dots), or fluorescent beads are useful as biolabels [96, 97]. Each has drawbacks. Q-dots are small in size and photostable with tunable optical properties. Yet, their quantum efficiency lags when compared with organic dyes. Real-time monitoring might be limited by their blinking emission. Furthermore, the UV range required for Q-dot excitation might be harmful to biological species. Upon UV excitation, highly toxic Cd^{2+} ions are released as a consequence of surface degradation. The release of Cd^{2+} is detrimental for living cells. Many methods were designed for the production of such fluorescent colloids but the focus of this review is on fluorescein isothiocyanate (FITC)-encapsulated silica-based nanoparticles. Silica has been widely chosen for both industry and laboratory research because of the reasonably close refractive index matching with organic solvents such as chloroform, cyclohexane, and hexadecane. In the early 1990s, Van Blaaderen and Vrij developed a facile method to produce FITC-silica through two major steps [98]. First, FITC was covalently bound to a silane-coupling agent, 3-aminopropyltriethoxysilane (APS), and formed the FITC-APS molecule, as shown in Scheme 7.

Second, the FITC-APS reaction product was incorporated in a Stöber mixture consisting of water, ammonia, and TEOS. By sequential addition of TEOS, silica either with a thin fluorescent shell or an inner layer was produced. The latter approach retards dye leakage and photobleaching. A series of reports using a similar procedure to obtain fluorescently labeled particles was recorded [99, 100].

Polypeptide composite particles

Clickable/amine initiator cores: preparation by surface functionalization and product characterization

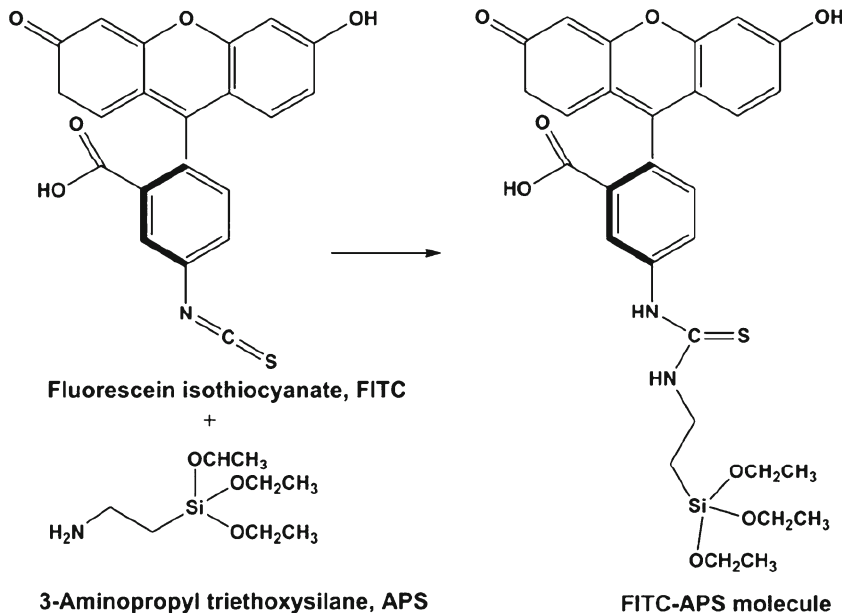
This section will outline some general aspects of surface tailoring and, afterwards, will focus mainly on amino-decorated silica surfaces. The attachment of functional groups on the surface of particles governs their solubility and chemical functionality. The groups or the molecules attached, either by physical or covalent bonds, should provide a stable colloid suitable for further chemical modification. As mentioned in previous sections, one of the most common routes to

functional materials is silica coating. Naked metal nanoparticles are in some cases very air/moisture sensitive and a thin layer of silica protects against oxidation. Furthermore, the silica surface has terminal –OH groups which can be easily reacted with other molecules by a simple chemistry. From this perspective, particles consisting of a magnetic core and a silica shell [50, 101] have received particular interest in terms of their magnetic responsiveness and controllable interparticle interactions by tuning the shell thickness and their biocompatibility [102]. The silica surface which has a negative charge in the 6–7 pH range is a convenient model to mimic the behavior of the negatively charged biomolecules in physiological conditions [103]. Coatings with double layers of silica, prepared by sequential addition of TEOS, led to materials suitable for the magnetic bioseparations and drug delivery. The first layer protects the core against degradation or etching in rough conditions and the external one can be etched in basic or acidic conditions to a porous structure. Consequently, enhanced properties can be obtained such as high surface area. In this order of ideas, Sen et al. [104] discovered a jump from 25 to 250 $\text{m}^2 \text{g}^{-1}$ surface area while Deng et al. [105] reported 365 $\text{m}^2 \text{g}^{-1}$. On the other hand, the silica shell can screen the magnetic response of the composite, causing an increase in coercivity [106]. Thus, control over silica coatings is essential.

Various functional groups can be attached to the surface such as –SH, –COOH, –N₃, –CHO, –Br, vinyl substituents, biomolecules (e.g., oligonucleotides), and polymers [107–110] but in the next lines the focus will be placed on amine-functionalized particles used as initiators in the *grafting from* method. The most widely used amine precursor is APS. The activation of the silica surfaces with APS is usually carried out in organic solvents [111]. The silane-coupling agents react with the silanol groups to yield an amino-functionalized surface. In order to lower the cost of production, surface modification in aqueous media was also devised. The latter approach involves the hydrolysis of the amino precursor at pH 3 and, afterwards, the condensation with silanol groups, resulting in siloxane bridges [112]. Even though the chemistry behind aminoactivation is well established, it still suffers from the difficulty of controlling the loading and poor reproducibility. An issue in using organic solvents is the water content. Assink and Kay [113] have shown by ¹H and ²⁹Si NMR that the rate of hydrolysis substantially exceeds that of condensation. Thus, a safe approach to water-free silica suspension involves azeotropic distillation followed by amino-functionalization using anhydrous solvents. A recent review by Rother et al. discusses the pros and cons of the generally accepted amino-silanization mechanism for the surface activation [114].

Applications of hybrid particles may require either densely [115] or sparsely [116] activated surfaces. A crowded assortment of amine groups can be obtained either by the reaction of silica particles with amino silanes [117] or the co-

Scheme 7 Sketch of the FITC-APS molecule formation



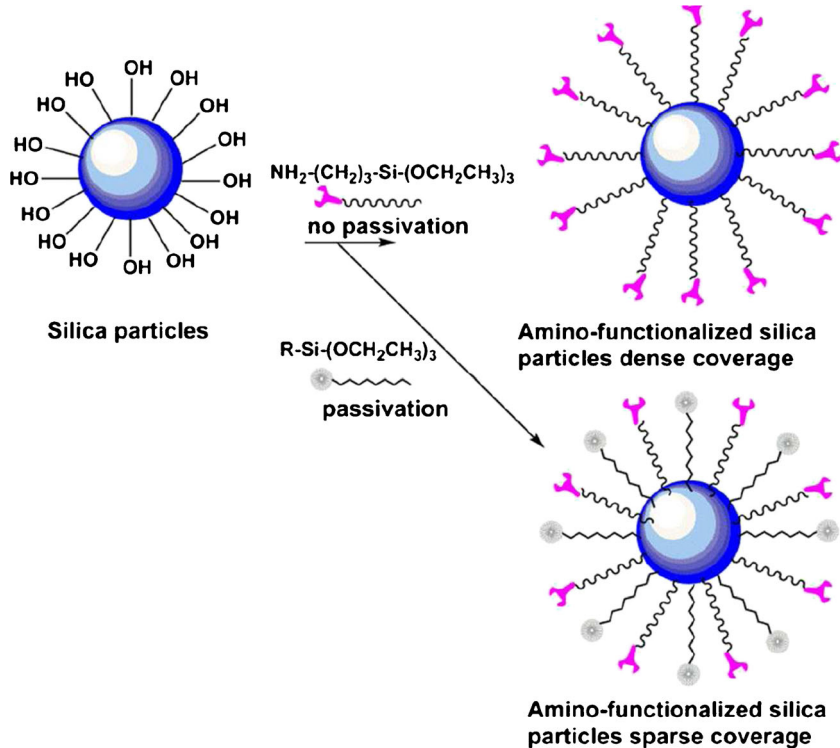
condensation between the silicate and amino precursors [118]. When preparing dense amino-grafted surfaces, one requires a method designed with the competition between amine–amine and amine–silanol groups through H-bonding in mind. Better control on amino sites is provided by co-functionalization. This process ensures the separation of the amine functional moieties by capping the free silanol groups, as shown in Scheme 8.

In order to manipulate the loading of functionalities on the surface, researchers have used various approaches. Mixtures of amino silanes and alkyl silanes such as APS and methyl trimethoxysilane (MTMS), respectively, were considered the easiest way to assess control over the grafting density [111]. Hydrolyzable templates placed on silica favored low loading (less than 0.2 mmol NH₂/g product) [119]. Yet, after hydrolysis, the silanol-free groups are available for interaction with amine. The molecular imprinting and thermolytic deprotection of carbamate silica to the corresponding amino silica have yielded particles with less than 0.23 or 0.27 NH₂ g⁻¹ of the matched-set material [120]. The Jones group devised a unique method involving the immobilization of the bulky tritylimine [121]. Deprotection in acidic conditions afforded the creation of spaces between amine groups [121]. They also used benzyl spacers. Still the amine–amine and amine–silanol interactions were assumed to be reduced or eliminated but no quantitative assay of OH groups was performed to verify the assumption [122]. Several groups have used only APS without any passivator and they have calculated the amount of the amino precursor per surface unit based on the concentration of the particle suspension and total surface area of the colloidal particle; for an introduction to literature, see an old and a recent report [8, 123]. The key factor in the activation–passivation seems to be the length of

the two species. A long amino silane and a short alkyl silane can reduce or eliminate the amine–silanol interactions but the H-bonding between adjacent amines is still present. The amino end-capped chains can bend and can hinder other functional groups or become inaccessible for further molecule attachment. Consequently, a better approach to arrest such interactions will be the use of activator–passivator with comparable lengths. Such a method was devised by the Heise group in the late 1990s [6]. They prepared 1-bromo-11-(trichlorosilyl)undecane and 1-trichlorosilylundecane, then grafted them to flat silica surfaces. The conversion of terminal bromine groups to azide by reaction with sodium azide, NaN₃, followed by the reduction in the presence of LiAlH₄ yielded a surface covalently grafted with amino groups [6]. If the reduction to amino groups is not performed, the azide-functionalized particles can be further used in click chemistry coupling. The same approach based on the activators and passivators of similar length was used by Soto-Cantu et al. for a convenient preparation of amino-functionalized particles with different and quantifiable grafting densities [111].

The quantification of amine function is necessary in order to maintain a control over subsequent steps. Several methods such as fluorometry [124], spectroscopy [125], and colorimetry [126] have been reported. Most of them involved only flat inorganic or organic surfaces. Some are more time consuming and expensive due to the cost of fluorophores. The success of these techniques in the quantification of amine moieties relies on their reactivity, their stability, and their capability to attach labels and probes. Microscopy (electron and light) and spectroscopy (e.g., X-ray photoelectron spectroscopy) give useful information about surface composition and binding energies, but their efficacy is limited mostly to flat surfaces. Moreover, a covalent attachment between the primary amino group and the

Scheme 8 Schematic illustration of the surface reactions involved in the formation of dense (*top*) and sparse (*bottom*) coverage with amino functional groups



label, in some cases, is required. A standardized, fast, inexpensive, and accurate determination of the amino moieties grafted on silica beads or other spherical surfaces is still under perfection. Recently, Coussot et al. [127] and Noel et al. [128] quantified the protonated groups NH_3^+ with Coomassie Brilliant Blue and Orange II, respectively, as the colorimetric reagents, but applicable to polymeric surfaces. Chen and Zhang devised a fluorescent Fmoc-Cl method which was found to be 50 times more sensitive than the UV assay [129]. They have shown that the pendant amino groups from the silica particle surface produced stronger fluorescence than a smaller amine freely dissolved in solution. A facile and inexpensive zeta potential method to determine the amino grafting density was proposed by Soto-Cantu et al. [111]. Thermogravimetric analysis (TGA) is another convenient resource researchers exploit in amino assay. Devised by Bartholomé et al., the method uses the weight loss percentages which ultimately are converted to the grafting density [130]. Other groups have proposed improvements but overall Bartholome's approach remains the milestone [131].

Synthetic shells: polypeptides and their N-carboxyanhydride precursors

The most economical and practical method for synthesis of polypeptides, especially homopolypeptides with long chains, is the polymerization of α -amino acid N-carboxyanhydrides (NCAs) [132]. These amino acid precursors were discovered by coincidence when Hermann Leuchs attempted to purify N-

ethoxycarbonyl or N-methoxycarbonyl amino acid chlorides by distillation and, at first, they were called Leuchs anhydrides [133]. Even Leuchs abandoned his work in this field because of disbelief in the existence of covalent polymers with molecular weights higher than 10,000 Da. Curtius [134] and Wessley and Sigmund [135] used primary amines, water, and alcohol as initiators and reported for the first time high-molecular weight polypeptides. These reports helped the international community of researchers to acknowledge Staudinger's concept of covalent macromolecules.

The ring closure of NCA with phosgene was pioneered by Fuchs by phosgenation of the α -amino acid in an aqueous solution [136]. The method, widely used, was modified over the years [137]. Suspension of α -amino acid in an anhydrous inert solvent such as dioxane or tetrahydrofuran and passing in the gaseous phosgene with stirring until complete dissolution of the acid led to a higher yield of NCA. Control over the amount of the dangerous gas release was achieved by bubbling it into a solution of ammonium hydroxide [138] or by using derivatives such as diphosgene [139]. The phosgene approach has several disadvantages. Besides its high toxicity, phosgene generates a high amount of HCl as a by-product, which can lead to further side reactions during the NCA polymerization. Consequently, the complete removal of HCl from NCA mixture is essential. Because the anhydride ring is very sensitive to moisture, the most common route to pure NCA is recrystallization performed in an inert atmosphere and with anhydrous solvents. Another method, such as rephosgenation, was proposed by Dorman et al. [140]. An

important contribution to the field of NCA synthesis was pioneered by Daly and Poché who substituted phosgene with triphosgene, (bis(trichloromethyl chloroformate)). The probability of side reactions was greatly decreased because only 1/3 equivalent of triphosgene delivered in situ was enough to close the NCA's ring in high yield [141]. The mechanistic route involved in the preparation of the polypeptides using triphosgene is depicted in Scheme 9.

Wilder and Mobashery also used triphosgene at room temperature [142]. A novel approach in the NCA purification was introduced by Poché et al. [143]. Cold, oily NCA mixture prepared in ethyl acetate was rinsed with icy water, neutralized with an icy solution of the sodium bicarbonate and finally dried with anhydrous MgSO₄. The stability of NCA toward cold water runs against the common belief that the NCA cannot tolerate water, which is true at room temperature. Poche's method allows the decrease in the number of recrystallizations which also improves the yield. Because the field of NCA polypeptide precursors grew rapidly, only representative work has been cited.

The work on the kinetics and the mechanism of NCA polymerization was comprehensively reviewed by Szwarc [144]. NCAs have several reactive sites that make the polymerization complicated. The carbamoyl (C-2) and carbonyl (C-5) are electrophile centers while NH (3) and α -C (C-4) are nucleophile sites, as shown in Scheme 10 inset. The polymerization path will depend mostly on the initiator's nature, nucleophilic or electrophilic. One major advantage of NCAs for polypeptide synthesis is the ring's capability to combine the activation of the C-5 carbonyl with the protection of the amino group. The activation of CO (C5) by the acylation of amino groups occurring at room temperature or even lower

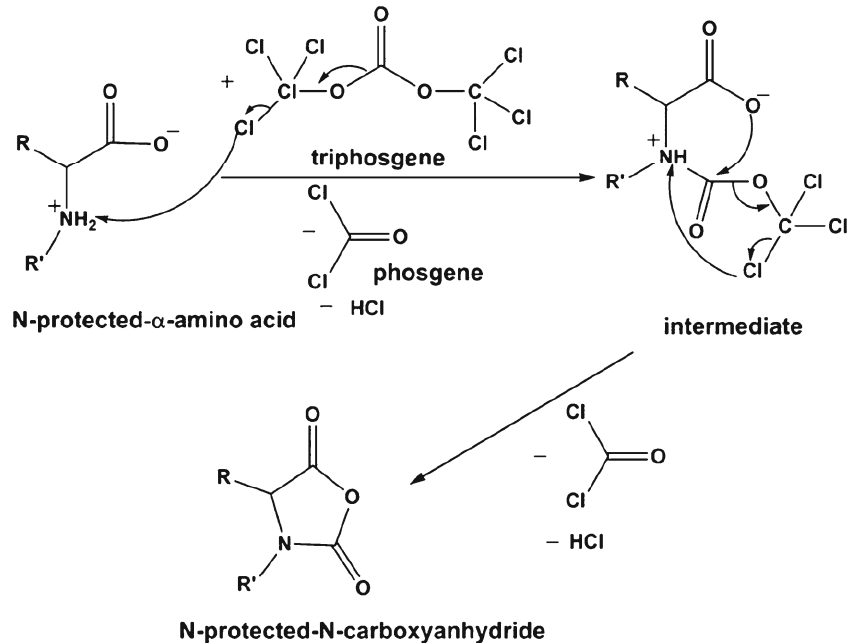
can yield oligomerization products very difficult to separate from the desired polypeptide. Although reports of using N-unsubstituted NCAs have appeared, the route did not attract large interest [145]. NCAs are not too unstable for easy storage over long periods of time, and water traces attached to the crystal surface through H-bonds can initiate the polymerization in the solid state.

In order to overcome some of these complications, NCAs can be either subjected to N-protection chemistry or protected amino acids can be used in their synthesis. The attachment of an electron-withdrawing group to the nitrogen lowers its nucleophilicity in such a way that the reaction with phosgene or its derivatives is not favored in mild conditions. In an insightful 100th anniversary review on NCAs, Kricheldorf compiled the routes to N-protection: cyclization of N-protected amino acids and attachment of a protecting group to a preformed NCA [146].

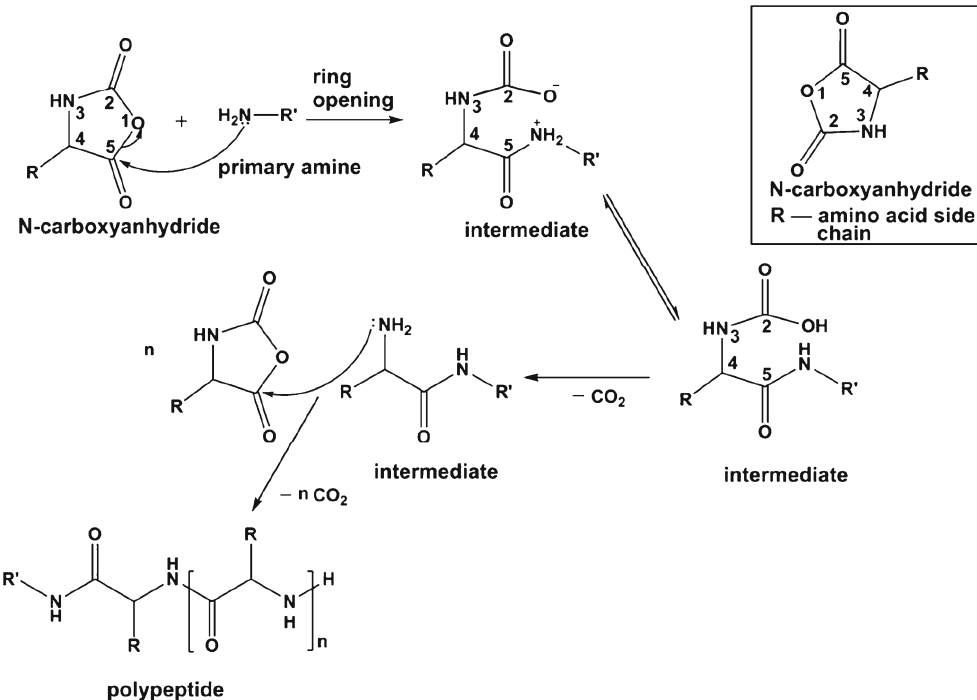
Since the beginning of the 1940s, polypeptides synthesized by the ring-opening polymerization of the corresponding NCAs have served as models of natural polypeptides and proteins to investigate the relationship between their primary and secondary structures. Polypeptides can adopt a multitude of stable secondary conformational structures depending on the nature of side chain substituent. The best known are random coil, β -sheet and α -helix [147].

Many studies have been devoted to the elucidation of the NCA polymerization mechanism. NMR and IR spectroscopy have been the most widely used analytical methods to detect the polymerization intermediate adducts and final products. Kricheldorf has published an important volume of work dedicated to the polypeptide formation mechanism, which is summarized in his review [148]. The most common

Scheme 9 Schematic of the synthesis of α -amino acid N-carboxyanhydrides, NCAs, with triphosgene. Adapted from reference [141]



Scheme 10 Schematic of the initiation and growth steps involved in ring-opening polymerization of NCAs initiated by a primary amine and the structure of NCA (inset)



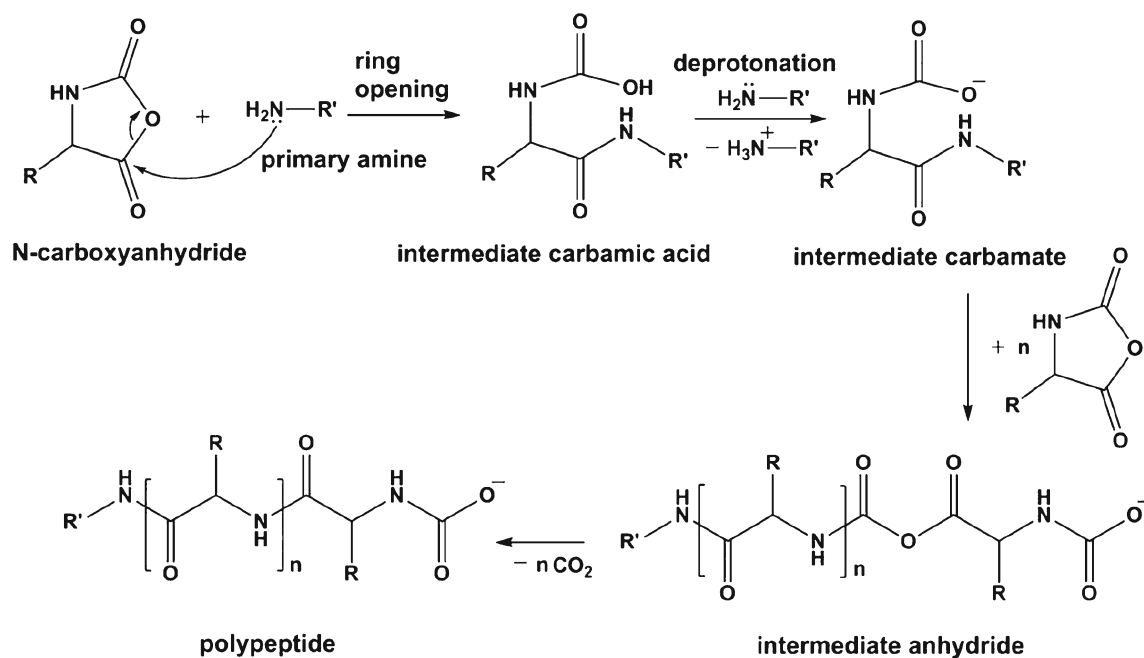
mechanism is through amines, whether primary, secondary, or tertiary. The first NCA polymerization to be initiated by amino groups was reported by Fuchs [136] and [135]. Kinetic studies were conducted by Waley et al. on the polymerization of sarcosine NCA [149]. The rate of propagation was followed by the increase in the CO_2 pressure at constant volume. The titration of terminal amino groups at the onset of polymerization indicated the absence of termination and, hence, the living character of the process. These findings were supported at that time by other researchers on other polypeptide-based systems [150]. Scheme 10 displays a schematic of the primary amine mechanism. The amine group of the initiator attacks the C-5 of the NCA monomer. The nucleophilic attack induces the ring-opening and, further, the decarboxylation of the intermediate unstable carbamic acid or its zwitterion [151]. The newly formed adduct will attack another nearby NCA molecule.

Study of the initiation by primary and secondary amines of isotopically labeled NCAs [152] showed that decarboxylation occurs at C-2 of the intermediate. This step was not demonstrated as the rate-determining process. The reaction should depend either on the intermediate formation or on the ring-opening between C-1 and C-5 [153]. The NCA monomer feeds the growth of the living polymer. At a specific monomer to initiator ratio, M/I, the chains should grow at the same time, assuming rapid initiation compared to propagation. The fast initiation is achieved with rapid addition of strong nucleophiles. The formation of the polypeptide can follow another pathway if the primary amine initiator is strong enough to deprotonate the intermediate carbamic acid, yielding a new adduct which further reacts with the NCA monomer and

forms an intermediate anhydride (Scheme 11). Decarboxylation of the intermediate anhydride enables the formation of the corresponding polypeptide.

Kricheldorf gave a critical overview on the previous work and used MALDI-TOF mass spectrometry among other techniques to better identify the end-group combinations [154]. Mass spectroscopy does not necessarily determine accurately the molecular weights and molecular weight distributions of the polymer, but qualitatively it does offer a picture of the distribution [146]. The polydispersity index (PDI) depends strongly on the polymerization medium and on the solubility and secondary structure of the growing polypeptide chain. Secondary reactions occurring during polymerization retard the propagation mechanism enabling the termination. Broad [146, 155] and low [146] PDIs were reported accounting for the aforementioned reaction conditions. Mostly poly(alkyl-glutamates) and poly(N-protected-L-lysine) were investigated but also other amino acid NCAs [156]. Optimum preparation of long chains with low PDIs can be achieved from soluble α -helix forming polypeptides and lowering the temperature to the freezing point of water [157]. Therefore, in NCA polymerizations initiated by primary amines, it is challenging to control the chain-end functionality and reactivity. The absence of side reactions results in a true living polymerization and the amino end-group is stable over a long time once the polypeptides are isolated as solids, as shown by Kricheldorf [146].

The inherent problem in conventional NCA polymerization is the poor control over the reactivity of the growing chain due to side reactions. An important contribution in this field was brought by Deming's group. They used transition metal



Scheme 11 Schematic of the initiation and growth steps involved in ring-opening polymerization of NCAs initiated by a primary amine through the carbamate mechanism

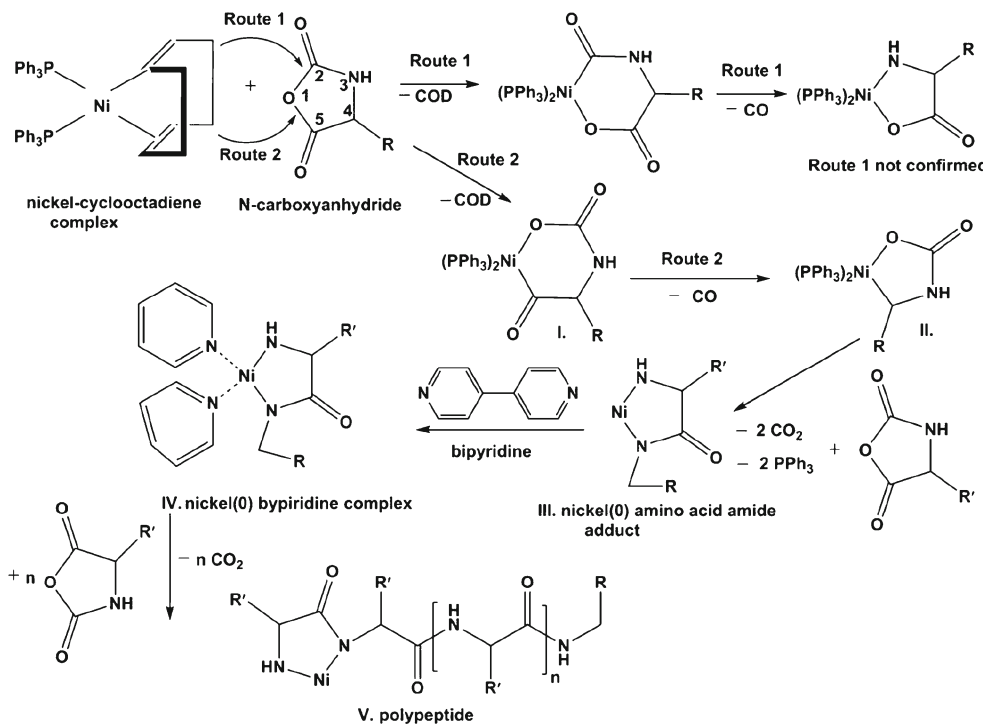
complexes as active species to control addition of NCA monomers to polymer chain ends. In order to increase both the reaction selectivity and efficiency, metal complexes such as zerovalent nickel [158] and cobalt [159] were used as catalysts in ROP of NCAs. The manner in which these metal complexes react with NCAs is similar. Scheme 12 illustrates the N-carboxyanhydride polymerization initiated by the Ni(0) complex.

The oxidative addition reactions intermediately by a NCA molecule yield six-membered amido-alkyl metallacycles (I). Further, these cyclic intermediates contract to a five-membered ring upon addition of the NCA monomers (II and III). This process was explained to occur via proton migration from an amide group to the metal-bound carbon, thus liberating the chain end from the metal (III). Complexation with bipyridine of the nickel (0) amino acid amino adduct (III) yields a soluble complex (IV). This cyclic intermediate (IV) in route 2 was proposed as the active species capable of initiating the nucleophilic attack of the amido group on the electrophilic C-5 of the NCA [146, 160]. The large cycle formed as the result of the propagation could contract through CO_2 release. The amido-amidate propagating species (V) formed as a result of the proton transfer from the free amide to amidate group enables ring contraction. The end chain of the polymer becomes free and the metal chelate can migrate along the growing polymer [161]. Although some details of the mechanism remain to be determined, Deming's work spans a variety of preparative applications. Variation of the metal type allowed good control over the molecular weight

and PDI of poly(glutamate)s, and the use of the different NCA precursors resulted in a broad range of homopolypeptides. No less important are the many architectural copolypeptides designed by using metal chelate initiation; for a convenient entry to the literature, see references [146, 160].

The common theme of improving the classical amine-initiated polymerization initiators was also shared by other groups. Hadjichristidis conducted primary amine-initiated polymerizations of NCAs under high-vacuum conditions [162]. The high-vacuum approach allows an effective purification by recrystallization of both unsubstituted and substituted NCA monomers. The polymerization of γ -benzyl-L-glutamate NCA (BLG-NCA) in DMF under high vacuum was found to have a living character. The main conclusion drawn by the authors is that the side reactions in the amine-initiated mechanism result from impurities contained in the monomer. Furthermore, the continuous removal of CO_2 generated during the reaction drives the polymerization [162]. When the volume of the reactor used was smaller than that of CO_2 produced during reaction, the polymerization of NCA was incomplete. Low-polydispersity products (typically $\text{PDI}=1.06–1.1$) were obtained with predictable molecular weight but the method needs more insight on the chain-end characterization. In a recent report of Pickel et al., the preparation of the poly(o-benzyl-L-tyrosine), in DMF was performed both using high-vacuum techniques and glovebox environment [163]. Polymers prepared by initiation with 1,6-diaminohexane in the high vacuum followed the normal amine pathway, the termination occurring with DMF. Products prepared in the

Scheme 12 Schematic of polymerizations of N-carboxyanhydrides initiated by Ni(0) complexes. Adapted from reference [146]



glovebox showed initiation by both amine and activated monomer mechanisms and the termination yielded several species. Nano-assisted desorption/ionization time-of-flight mass spectrometry, provided the chain-end analysis and pointed to the end-group fidelity obtained via high vacuum [163].

N-trimethylsilylaminies were used for controlled ring-opening polymerization of NCAs by Cheng and Lu [164]. The unique feature of this technique is that the amine end-groups are obtained after cleaving the protecting trimethylsilyl end-group. A narrow distribution was achieved ($PDI=1.19\text{--}1.26$) and the ^{13}C NMR coupled with other mass spectrometry techniques determined the nature of terminal groups [164]. The same group has used N-trimethylsilylaminies to polymerize O-carboxyanhydrides [165]. In order to avoid the formation of NCA anions during the polymerization, Schlaad used primary amine hydrochloride salts as initiators [166]. Their goal was to inhibit the polymerization through the activated monomer mechanism, obtaining in this way macromolecules with low dispersity. Higher values of molecular weight were obtained for products when compared with those theoretically computed [166]; however, end-group determinations were not presented.

The identification of the terminal groups is also important from another point of view. For a long time, it was believed that polymers made by NCA ring-opening were linear, unless branching was intentionally desired. One paper stated otherwise [167] until Kricheldorf confirmed the *in situ* formation of the cyclic polypeptides along with the linear analogs [146]. Solvents with high dielectric constant (ε_r), high nucleophilicity, and donor ability such as pyridine ($\varepsilon_r=12.4$), DMF ($\varepsilon_r=36.7$),

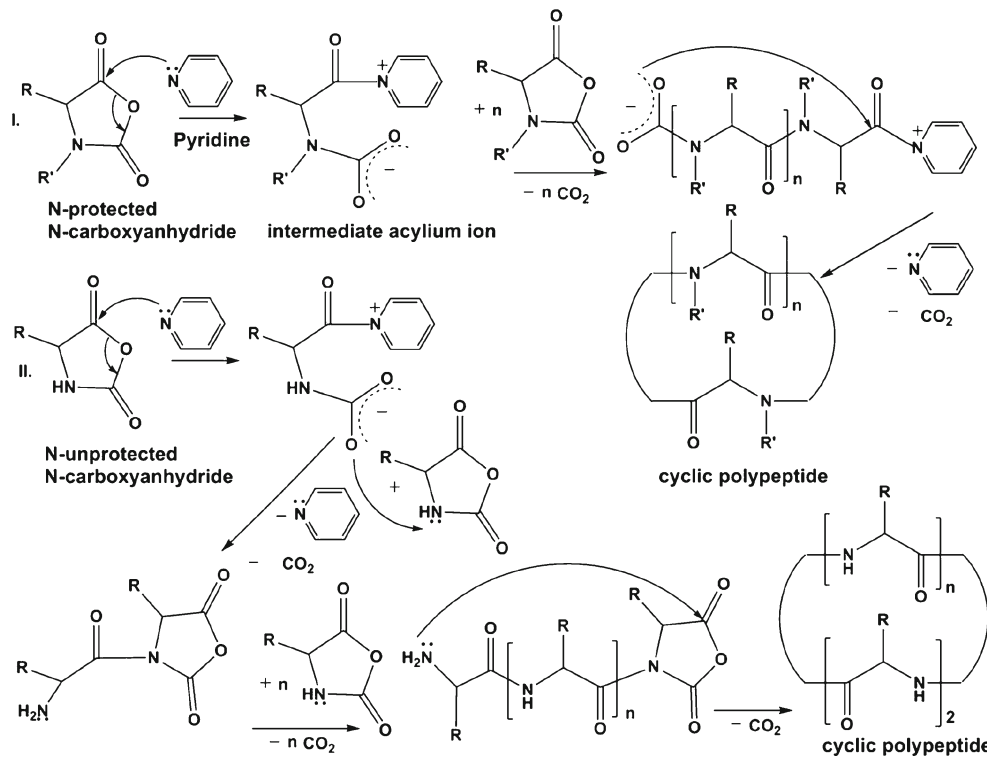
N-methylpyrrolidone ($\varepsilon_r=32$), and DMSO ($\varepsilon_r=46.7$) were found to catalyze zwitterionic polymerizations [146]. The Scheme 13 and Scheme 14 display the interactions between the polymerization species when the solvent involved is pyridine and DMF, respectively.

Consequently, the polymerization mixture might be a blend of mostly linear chains with cyclic “contaminations” when the synthesis of homo- and co-polypeptides is carried out in these solvents. Soluble polypeptides that adopt a random coil conformation showed a high tendency toward cyclization [146]. It has been known that traditional NCA ring-opening polymerization leads to low-molecular weight polymers [146]. Once removed (and usually discarded), the remaining high-molecular weight polymer is good ($M_w/M_n \sim 1.2$). Given the interest in deliberately making cyclic polymers, perhaps the low- M cyclic polypeptides ought to be retained rather than discarded. In any case, production of good-quality linear polymers for fundamental studies by the classic methods is easy if one accepts the loss of some material to the cyclic oligomers and the extra fractionation step. Even if the goal is to make co-polypeptides, one can tolerate the cyclic impurities at intermediate stages because they are unreactive towards added monomers.

Other techniques to uniform polymers were also reported. For a convenient entry to co-polypeptide, DNA recombinant approach and urea-assisted NCA ring-opening polymerizations literature see old and new references [162, 168–173].

To summarize this section, Scheme 15 highlights selected contributions in the field of living polypeptides. The cyclic arrangement shows how the field has progressed from emphasis

Scheme 13 General route of the pyridine-mediated ring opening polymerization of N-protected N-carboxyanhydrides via zwitterionic ionic intermediates. Adapted from reference [146]

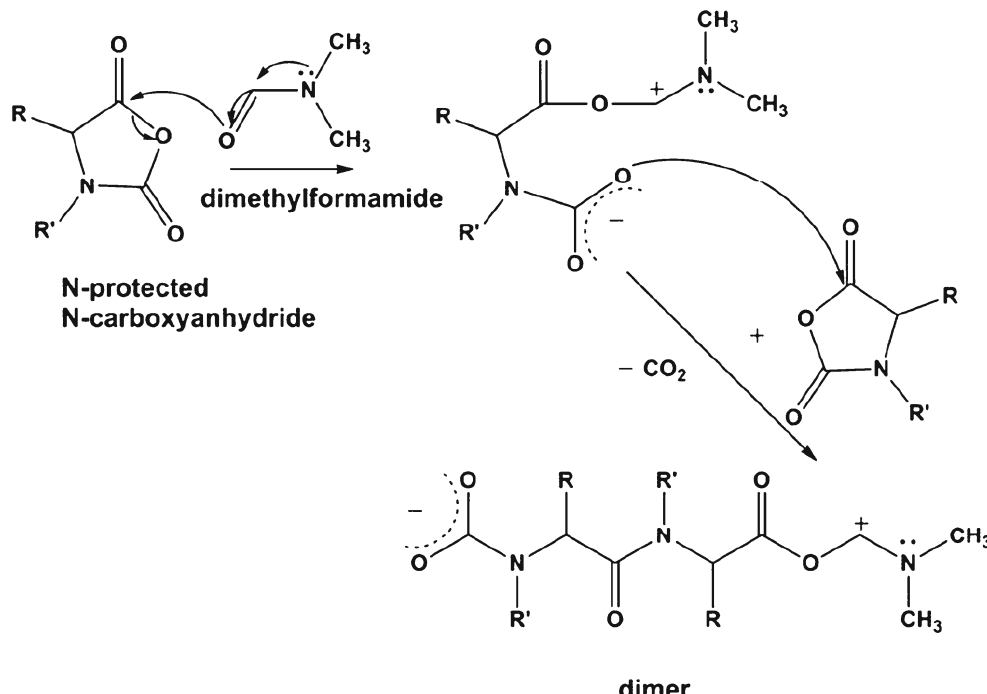


on high reagent and solvent purity and dryness to controlled polymerization methods using catalysts and back to even greater emphasis on dryness through high-vacuum technique.

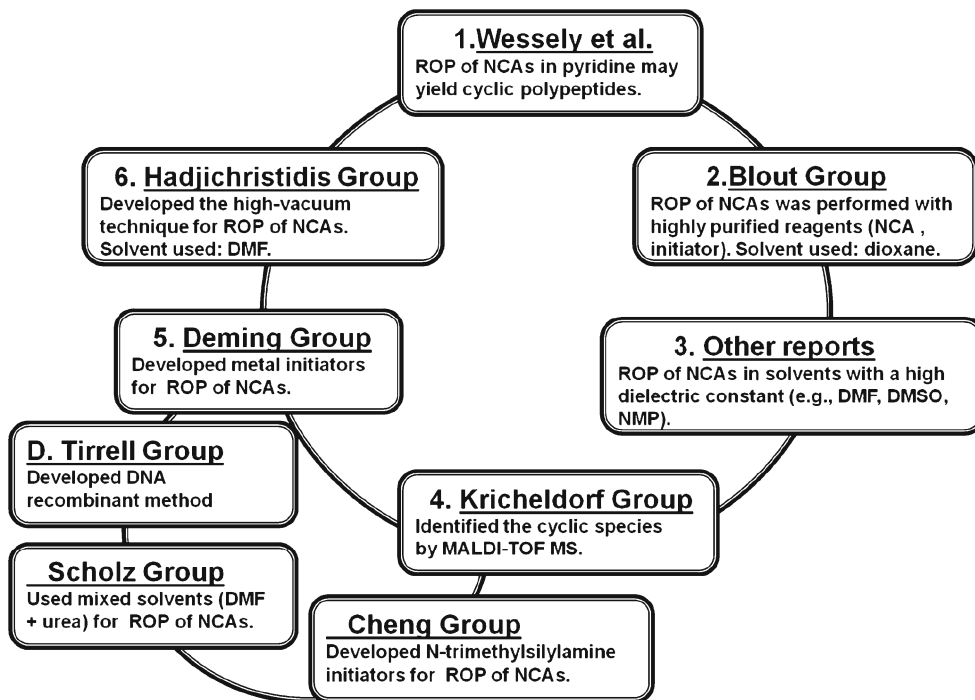
In the 1950s, Wessely observed complications in NCA polymerization using pyridine as solvent. Because the end-groups could not be identified, they suspected the polypeptides were cyclic. Soon afterward, Blout and collaborators reported

high molecular weight ($M > 10^6$) polypeptides using dioxane as the polymerization solvent. Their work is remarkable for the care taken to prepare high-purity reagents. Reports after Blout started to use solvents with a high dielectric constant such as DMF or DMSO. It is possible that these researchers were aware of the aggregation problem in dioxane, while solvents such as dry DMF and DMSO do not promote association [174]. The

Scheme 14 Schematic of the initiation steps of solvent (DMF)-induced zwitterionic polymerization of N-protected N-carboxyanhydrides. Adapted from reference [146]



Scheme 15 Brief history of polypeptide synthesis



road of ROP polymerization was then paved with more complications. One of them was the lack of adequate techniques to estimate the end-group functionality. Eventually, Kricheldorf was able to investigate the reaction mixture with MALDI-TOF. The living character of the ROP polymerization was proven but cyclic species were also identified, validating Wessely's suspicion. Kricheldorf emphasized that pyridine and DMF promote the ROP of NCA as a competing side reaction leading to cyclic polypeptides. Yet the intermediates in the DMF initiation were not identified as pointed out by Hadjichristidis. Small traces of dimethylamine derived from DMF can also be responsible for side reactions. In order to address some of the complications, Deming devised organo-metallic initiators. These polymerizations had a living character and are suited well to preparing block co-polypeptides, but PDIs did not improve consistently above those seen by earlier workers after fractionation. Hadjichristidis has closed the circle of history in polypeptide synthesis by developing the high-vacuum technique, which ensures dryness of solvents, but continued developments are almost certain to follow. After near a century of development, one has to marvel that the low PDI and high molecular weights achieved by earlier workers are not routinely surpassed. Some of the approaches do make the synthesis easier, though, and this contributes to the growth of the synthetic polypeptide field.

Routes to silica–polypeptide hybrids

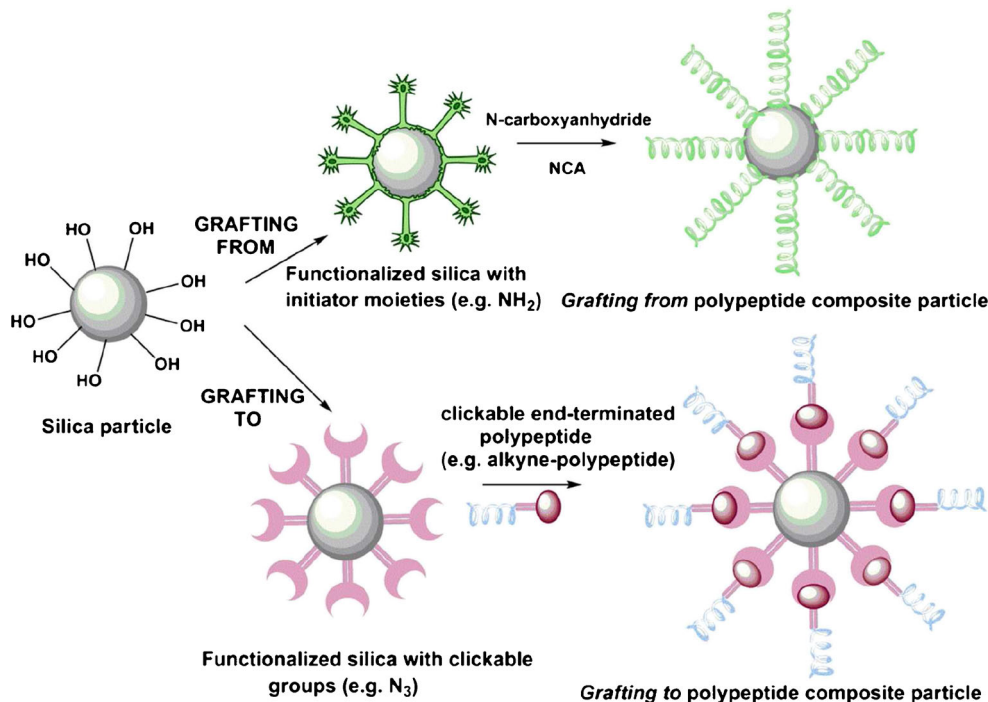
Although polypeptides are large molecules, especially in the extended α -helical conformation, it is not trivial to manipulate

them. Silica–polypeptide hybrids combine the many features of polypeptides, chirality, and its associated optical properties, plus the availability of sharp conformational transitions with the easy handling of colloid particles by sedimentation, filtration, electronic, or magnetic attraction. In this section, early reports on silica–polypeptide hybrids will be summarized and, as well, trends in present research. Methods used in hybrid material synthesis such as *grafting to* and *grafting from* will be compared and the shortcomings in designing the desired properties of the final product will be also addressed. The main steps involved in these two techniques are presented in Scheme 16.

Although this review treats particle-polypeptide attachment, many efforts have been dedicated to polypeptides deposited on flat surfaces by the classical ROP of the corresponding NCA or by vapor deposition to create polypeptide brushes whose layer thickness and roughness can be measured by ellipsometry, reflectometry, and atomic force microscopy [175, 176]. Researchers were devoted to controlling the surface grafting density, assessing the orientation of the polypeptide chains, growing multi-polypeptide layers, and most importantly exploring the conformational changes in response to external stimuli [177, 178].

The first polypeptide-coated particles were reported in 1970s by Dietz et al. [5]. They grafted poly(L-leucine) on amino-phenyl silica as a better support for initiation than *p*-toluidine. In 1980s, Tsubokawa et al. attached covalently PBLG on amino-, methylamino-, and dimethylamino-functionalized carbon black [7]. Their objective was to investigate the grafting percentage of polypeptide onto carbon

Scheme 16 Schematic illustration of the *grafting from* and the *grafting to* methods. Not drawn to scale



black having primary, secondary, and tertiary amino functionalities. About 12 years later, particles of improved uniformity were produced [8], as an extension to the colloid regime of efforts to produce star poly peptides [179]. Soon, beautiful colloidal crystals were obtained from PCBL-grafted silica upon improving the uniformity of the silica cores [180]. To limit the effects of polydispersity on the formation of colloidal crystals [181], and with a *grafting from* realization of the potential of particles bearing functional poly peptides, methods to control the grafting density were necessary. Equally important is the need to know the length of the polymer shell.

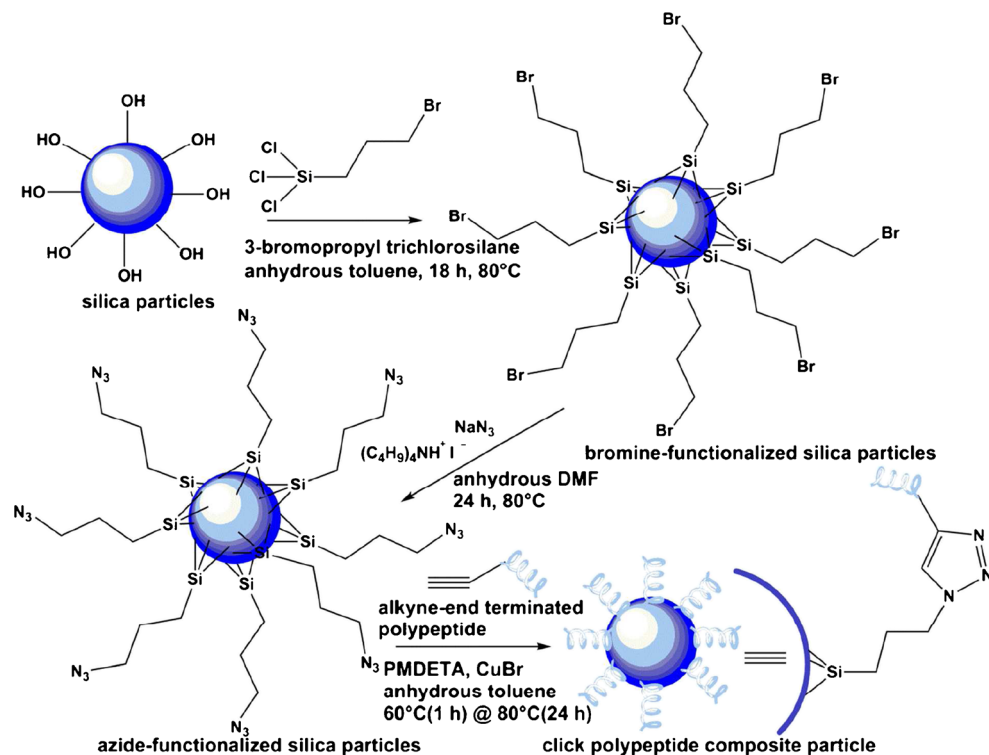
The *grafting to* method

The emergence of click chemistry, especially Huisgen 1,3-dipolar cycloaddition between azide and alkyne groups, has made possible the control over the length of polymer attached to the core. This is the major advantage of the *grafting to* method: well-characterized poly peptide chains, further attached to the functionalized surface of the core, produce a uniform shell. Another feature of click chemistry is the possibility to match the end-group of the preformed polymer with the reactive functional moiety grafted on the silica surface. The compatibility between the matching groups prevents interference with any other functional moieties on the silica surface or on the polymer. It also favors the fast covalent grafting step over the other competing processes (e.g., polymer chains can fold and cover the reactive surface). The chemoselective and fast *grafting to* method is also known for its tolerance to a broad range of functional groups [182,

183]. The most popular among all is the cycloaddition of an alkyne and azide groups via stable 1,2,3-triazole linkages, as shown in Scheme 17.

Click chemistry was involved from the very beginning in coupling premade polymers or biomolecules to peptides, proteins, nucleic acids, viruses, cells, sugars, and synthetic polymers, as reviewed by Binder and collaborators [184]. Several groups reported block copolymers made of homopolypeptides [185, 186]. Yet, few reports have appeared about click hybrid particles featuring a homopolypeptide shell or other synthetic polymer [187]. Balamurugan et al. grafted an α -helical hydrophobic PSLG to silica particles [188]. These particles formed stable dispersions in a broad range of organic solvents such as THF, chloroform, dodecane, and toluene. The molecular weight of the coupled polymer was calculated to be approximately 4,600 Da based on the monomer-to-initiator ratio and a repeat unit weight of 381 g mol⁻¹. Gel permeation chromatography (GPC) with multi-angle light scattering (MALS) measurement returned a much higher value as listed in Table 1, an indication that some initiator molecules were probably inactive or yielded small dead chains. At the same time, the Gupta group combined click chemistry and the ROP of NCAs to fabricate PBLG-, PLL-, and poly(L-glutamic acid) (PLGA)-grafted silica particles with a high grafting density. The methodology was extended to obtain co-polypeptide-grafted hybrids such as poly(L-lysine-b-poly-L-leucine) (PLL-b-PLLeu) silica particles [189, 190]. Recently, the Gupta group expanded their investigations on poly-L-arginine composite materials [191]. The molecular weights of the grafted polymers appear in Table 1.

Scheme 17 Schematic of the surface reactions involved in the preparation of polypeptide composite particles using click chemistry



Comparison of the results contained in Table 1 also helps to identify some drawbacks to the *grafting to* approach. Regardless of the available range of alkyne-amine initiators, control over the desired molecular weight of the polypeptide is still not evident. For example, propargylamine, one of the most common primary initiators used in click chemistry, is not reactive enough. The initiation step needs to be fast in order to enable the propagation and the growth of the nascent chains in the same time. The preparation of very short as well as very long polypeptides still remains a challenge. Lately, new initiators that are more reactive were developed and offered a

better control over polymerization. One of them, N-trimethylsilyl propargyl amine [164], also used by the Gupta group seems to give low-polydispersity polymers and molecular weights that lie closer to those predicted from the monomer-to-initiator ratio.

Even if the polymer has a well-characterized molecular weight, once grafted onto the surface, the loading on the particle still remains low. An optimum population of active functions on the surface that will allow higher polymer grafting densities can be obtained by using Heise's mixed functionalization approach described in “Clickable/amine

Table 1 Polymer name, ratio of the monomer to initiator, weight-average molecular weight, polydispersity, and the corresponding reference for several polymers prepared for click chemistry

Polymer	$[M]/[I]$	M_w			PDI	Reference
		Theoretical	Actual			
Alkyne-PSLG	12	4,600	8,480	1.15	[188]	
Alkyne-cbz-PLL	30	7,900	8,000	1.05	[190]	
Alkyne-PBLG	25	5,400	7,000	1.1	[190]	
Alkyne-p-methoxy-PBLG	30	7,400	9,500	1.08	[189]	
Alkyne-p-methoxy-PBLG	40	9,900	12,000	1.04	[189]	
Alkyne-PLGA	30	3,800	4,300	1.08	[189]	
Alkyne-PLGA	30	3,800	5,000	1.04	[189]	
Alkyne-cbz-PLL-b-PLLeu	25:15	8,400	8,000	1.06	[190]	
Alkyne-dicbz-p(L-Arg)	20	7,687	7,600	1.06	[191]	
Alkyne-dicbz-p(L-Arg)	10	3,870	3,800	1.11	[191]	

initiator cores: preparation by surface functionalization and product characterization” section [6]. A crowded shell may fail to undergo secondary transitions in response to the external stimuli. In order to illustrate the aforementioned attributes, Table 2 summarizes grafting densities obtained by the two groups for several click particles.

Another disadvantage in the *grafting to* approach arises from the difficulty and the costly protocol to remove the copper traces from the final product. Used in tandem with a ligand, the common *N,N,N',N',N"-pentamethyldiethylenetriamine* catalyzes the coupling reaction between the azide and the alkyne functionalities through stable 1,2,3-triazole bonds. Recently, sulfonated bathophenanthroline [189], specifically the copper in the salt form (e.g., CuBr, CuI), was also used as catalyst. The presence of the metal in the click colloid can exert cytotoxic effects on metabolism in living organisms, which hampers its use in biological applications. A step toward improving the utilization of this method was made by the innovation of the copper-free click chemistry. Biorthogonal reactions use components inert to the biological environment and employ several classes of reagents. One class of molecules, cyclooctynes, pioneered by Wittig and Krebs [192], reacts selectively with the azide groups at ambient temperature. The activation energy of the classical Huisgens [3+2] cycloaddition is high, 26 kcal mol⁻¹ [193]; thus, elevated temperature and pressure are required to accelerate the rate of coupling. The copper-free chemistry has a lower activation barrier, 18 kcal mol⁻¹ of ring strain [194]. Cyclooctynes have highly strained ring conferring them a higher reactivity at ambient temperature and pressure. Recent developments were directed to increase the reactivity and selectivity of the cyclooctynes. Jewett and Bertozzi [194] have presented an in-depth review of biorthogonal chemistry. The drawback of the copper-free click-to approach is the cost and complicated chemistry behind the synthesis. The future of this subclass of click chemistry is very promising in terms of the visualization of substructures in cells and conducting reactions *in vivo* (e.g., covalent labeling of biomolecules). The method will also allow the in-depth study of the cellular machinery. Recent reports used biorthogonal chemistry to prepare macromolecular self-assembling building blocks, polypeptide-g-polyhedral silsesquioxane (POSS) copolymers from a mono-

azido-functionalized POSS and poly(γ -propargyl-L-glutamate) (PPLG) [195]. The PPLG-POSS nanoparticles had superior thermal properties and better conformational stability compared to pure PPLG.

The *grafting from* method

Disadvantages of the *grafting to* method can be circumvented by using the *grafting from* technique. Historically the *grafting from* method was used as an exclusive tool to grow polypeptide brushes on planar surfaces such as silicon wafers. The ring-opening polymerization of NCAs was conducted in solution [6, 196, 197], melt [198], and by vapor deposition [199]. One of the most-used polypeptides for grafting was PBLG as described in the previous section. Early work demonstrated the successful growth of PBLG on spherical silica [8, 180]. Lately, the same group demonstrated the grafting of PCBL in a controlled fashion and opened the door to copolypeptide shells, as shown in Scheme 18 [200].

Control over the shell thickness could be assured by the sequential addition of the NCA monomer. The Heise group expanded the work on stimuli-responsive polypeptide-based silica hybrids and investigated the optimal conditions of polymerization to produce uniform shells [131]. Reactions carried out at 0 °C seemed to give a core–shell structure whose hydrodynamic radius increased proportionally with the BLG-NCA monomer addition. The same polypeptide was grown on silica encasing a magnetic (magnetite) nugget.

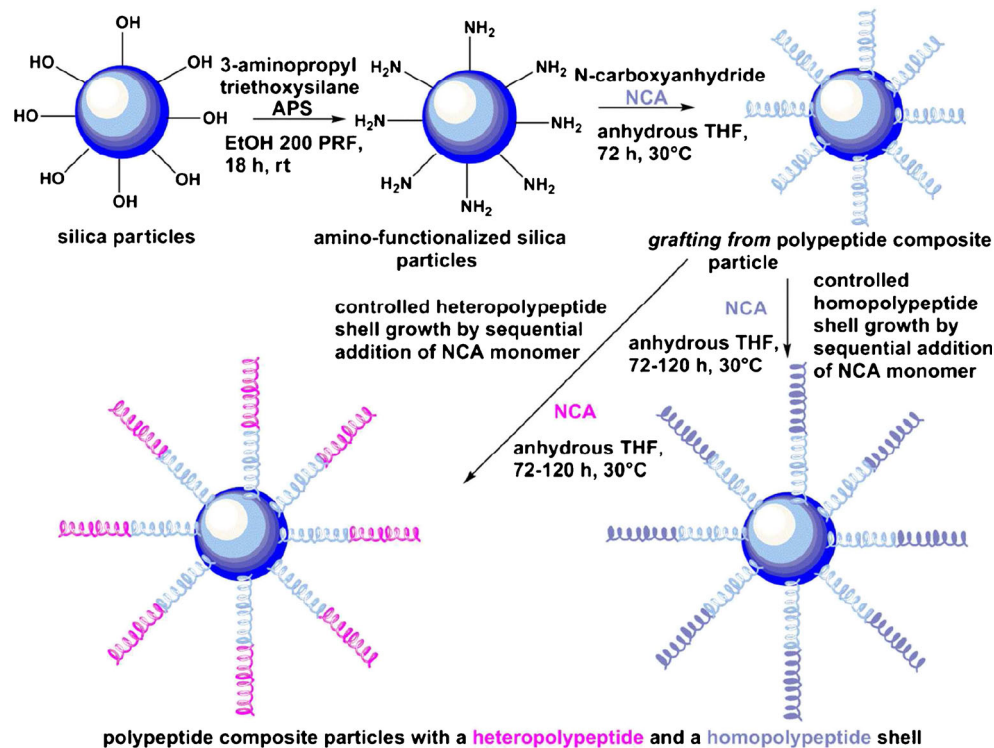
Even though the polypeptide loading on the *grafting from* particles is much higher than that on the click particles, the *grafting from* method suffers from several constraints which will be further addressed. First, the control over the grafting density still needs to be improved. For this reason, Soto-Cantu et al. used the tandem passivator/activator (e.g., MTMS/aminoethyl-3-aminopropyltrimethoxy silane and MTMS/3-aminopropyltrimethoxy silane) in an effort to avoid a densely polypeptide packed surface. Two sets of particles were prepared: one with PCBL as its shell and the other with a shell of PBLG [200]. Methods to demonstrate the packing nature of the shell are limited because the molecular weight of the polymer is not easily accessible unless the hybrid particle is subjected to a “haircut.” Information about the

Table 2 Hybrid particle name, core and overall size, weight loss, grafting density, and associated reference for polypeptide composite particles prepared by click chemistry

Hybrid particle	Diameter/nm (DLS)		Weight loss ^a %	Grafting density/ $\mu\text{mol m}^{-2}$	Reference
	Core	Core+shell			
Silica-PSLG	140±3	160±10	30	1.48	[188]
Silica-PLGA-30	22±3	37±3	25	0.427	[189]
Silica-PLGA-40	22±3	38±6	28.4	0.45	[189]
Silica-L-Arg	27±4	34±4	47	1.9	[191]

^a From TGA, attributed to the percent weight of polypeptide in the hybrid particles

Scheme 18 Schematic of the surface reactions involved in the preparation of the polypeptide composite particles having a homopolymer and a heteropolymer shell



“densification” of the shell was gathered by a combination of light scattering and computation methods based on the core–shell form factor [200].

$$I(qR) \propto R^6 \left[\frac{(m_1 - 1)}{2\pi} \left(\frac{3j_1(x)}{x} + f^3 \frac{(m_2 - m_1)}{(m_1 - 1)} \frac{3j_1(fx)}{fx} \right) \right] \quad (3)$$

In this equation, R is the outer radius of the polypeptide silica core–shell particle, $x = qR$, q is the scattering vector magnitude defined as $q = 4\pi n \sin(\theta/2)/\lambda_0$ (n is the solvent refractive index, θ the scattering angle, and λ_0 the wavelength in vacuum), and j_1 is the first-order spherical Bessel function given by $\sin(x)/x^2 - \cos(x)/x$. The relative refractive indices were expressed as $m_1 = n_1/n_0$ and $m_2 = n_2/n_0$ with n_0 , n_1 , and n_2 the refractive indices for the solvent, the shell, and the core, respectively. The term f designates the fraction belonging to the core from the total dimension of the particle: $f = (R - t)/R$ (t is the thickness of the shell). Well-solvated particles can be modeled using the refractive index contrast between the solvent, the shell, and the core [201]. Suspensions of PCBL silica particles in pyridine showed a near agreement between their radius measured by DLS and SLS (dynamic and static light scattering, respectively) suggesting good solvation, but with hydrodynamic screening, of a shell that was not densely packed. Using refractive indices of 1.507 for the pyridine solvent, 1.544 for the PCBL shell, and 1.445 for the silica core [200], there seemed to be adequate contrast to detect the sizes of both core and shell. Under these conditions and

assuming a hypothetical suspension containing only PCBL shell without core, light scattering at finite angles should return different values for both R_{SLS} (core–shell) and R_{core} (silica). The results did not reflect this trend, pointing once again to good solvation of the shell. Yet, this qualitative assessment could not associate the apparent thickness of the shell with polypeptide length even under the assumption that polypeptide is oriented perpendicular to the core surface. Small-angle neutron and X-ray scattering may prove more fruitful for evaluation of the shell thickness.

The continuous reactivity of the chain ends was demonstrated by sequential addition of BLG-NCA monomer using weight loss from TGA to follow the increased shell mass after each addition [200]. These results were confirmed by DLS. The lower grafting efficiency could be explained by the formation of untethered polymer in the polymerization mixture. This aspect was also noted by the Heise group [131]. The growth of the copolymers made of homopolypeptides on silica spheres was assessed. The importance of washings to remove the free, untethered polypeptide was reflected in the thermogravimetric curves. Approximately 25 % weight loss difference was recorded between the unwashed and the washed sample. The reactions conducted at various temperatures (0 and 20 °C) showed good control over the shell thickness, especially at 0 °C. This is in agreement with the findings that at 0 °C the NCA does not react with moisture.

Determination of the molecular weight of the homopolymer grown on the surface poses challenges. The most popular technique first requires etching of the silica

cores by hydrofluoric acid, HF, similar to the extensively used treatment of silica wafers [202]. HF is a weak acid and its use to cleave the polypeptide shell relied on the reasonable assumption that HBr, a stronger acid than HF, does not degrade polypeptides (however, see Fasman et al. [203] who found that high-M PCBL was degraded in the presence of HBr/CH₃COOH). To date, no detailed study has been conducted to determine the effect of etching conditions on the polypeptide shell of hybrid particles. The Heise group was the first to combine molecular weights from GPC and mass of shell polymer from TGA to determine the number of polypeptide chains on a particle (0.4 chains/nm² or 2.5 nm² “parking area” per chain) [131]. They obtained PBLG molecular weights from 7,700 to 20,100 Da for polymerizations conducted at 0 °C. The values for polymerizations performed at 20 °C were similar (8,700 to 20,100 Da). The polydispersity indexes were 1.4 (0 °C) and ~1.3 (20 °C). The authors claimed that lower temperatures are better, although the difference in molecular weights seems to be small. The polymerization conducted at 20 °C seemed to favor slightly lower PDIs. Some research groups have shown that polymerization in solvents such as DMF as Heise used can initiate the polymerization of the NCA, consequently competing with the initiation by the amino groups. The Heise group brought another important contribution to this field by engineering hybrids carrying a copolypeptide shell.

The stability of polypeptide-based silica hybrid dispersions is important in potential applications such as drug delivery. Soto-Cantu et al. aged PCBL–silica hybrids over 1 year after fabrication. According to DLS and SLS measurements, the particles tended to aggregate slowly, a prerequisite for the interdigitation of the shells, which offers certain opportunities (such as the creation of locally ordered phases). Sonication over 30 min reversed the aggregation: particle size was similar to that recorded just after preparation. The downward tendency of μ_2/T^2 , the DLS size polydispersity index from cumulants analysis, could be explained by the presence of the aggregate particles that could not be separated by sonication. The polypeptide seemed to survive the treatment for the aggregate breakage. Liu et al. sonicated their PBLG-SiO₂-Fe₃O₄ composite particle in DMF for 36 h to test the presence of the polypeptide on the magnetic silica surface [204]. This kind of information can be supplemented by thermogravimetric investigation. Ostlund and Striegel have shown that prolonged sonication of PBLG alters the chains [205]. The scission was noted to occur preferentially on the backbone between the weaker C–N bonds than the C–C or the side chain C–O bonds. The molecular weights dropped to less than half their initial value, but the polymer retained its helical conformation. It is not clear how the sonication affected the grafted polypeptide on the magnetic silica surface of Liu et al. or the particles “de-aggregated” by Soto-Cantu et al. Zhigang et al. have produced poly-L-alanine-grafted silica-coated magnetite particles for

hydrophobic targeted drug delivery. The hydrophobic interactions between the poly-L-alanine chains and ibuprofen, the drug model, suggested that these magnetic particles can be considered effective drug carriers [206]. No attempt was made to evaluate the molecular weight of the shell and the grafting density. No attempt was made to evaluate the molecular weight of the shell and its grafting density; however, drug loading likely depends on these parameters.

Layer-by-layer assembly of oppositely charged polypeptides

Although this review is devoted primarily to covalently attached shells, layer-by-layer (LbL) assembly has been exploited by Caruso and collaborators to adhere polypeptides noncovalently [207]. The efficiency of this method for capsule production justifies a few words. This technique relies on the electrostatic interactions between layers of oppositely charged polypeptides which are sequentially deposited on a silica sacrificial template. In this manner, the charge is compensated at each layer [208]. The LbL method has the advantage of controlling the capsule dimensions [207]. Engineered as drug carriers, these capsules must be small and flexible to travel through the circulatory system’s tiny vessels [209] without obstructing the blood stream. The LbL polymer assembly is not limited only to the electrostatic or the zwitterionic interaction. Lately, the LbL assembly was expanded to H-bonding [210] and also on the DNA–DNA hybridization [211]. The continuous development of click chemistry enabled the LbL deposition of the click functional group “matched” polymers [212]. Once the desired number of layers is loaded on the sacrificial silica, the core template is removed by etching with HF. Afterwards, the capsule can be loaded with drugs for release purposes. Initially designed with one single void, the morphology of the capsules was adjusted to create sub-compartmentalized micro-reactors, called capsosomes, by using liposomes [213, 214]. The Caruso group took one step further in the field and produced crosslinked PLGA particles. The procedure employed positively charged amino-functionalized mesoporous silica particles which were further loaded by LbL deposition with PLGA carrying cysteine residues [215]. Further, the final composite particle was obtained by disulfide crosslinking and the silica template removal. The polypeptide particles were found to degrade under cytoplasmic conditions and were stable under physiological conditions making them promising candidates as therapeutic carriers.

Recent developments, future trends and applications of polypeptide-based silica hybrids

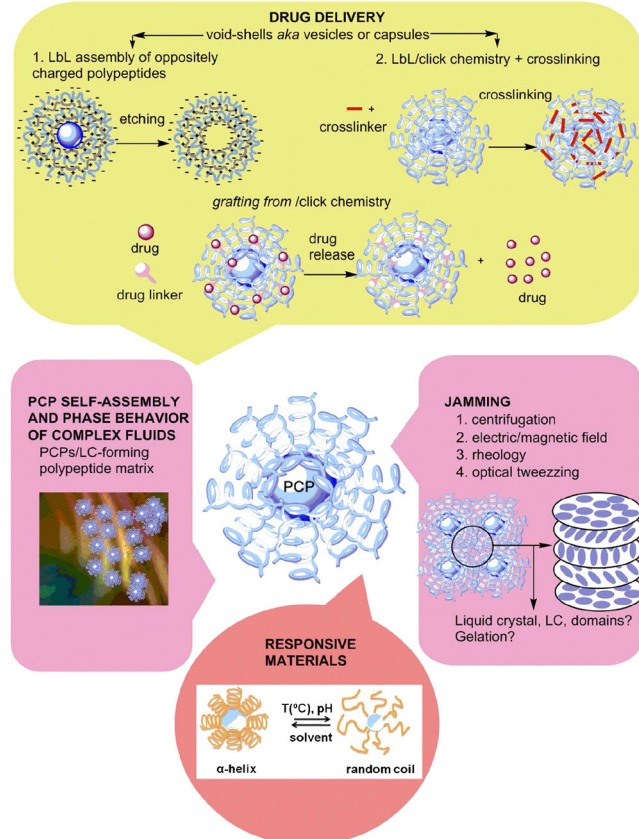
Many other proteins can form particles reminiscent of viruses in their overall structure but the PCPs have the advantage of sequence simplicity. Capsid structures resembling virions

have great potential for vaccines that could augment or perhaps replace therapeutic monoclonal antibodies used in some disease prevention treatments [216]. A well-defined core and a shell that can be adjusted to the intended shape and thickness makes PCPs attractive models to understand the interplay of forces between viruses and the living cells within the body. Moreover, such capsids or void-shells, as presented in Scheme 19, can be also obtained from PCPs by etching the core with HF or NaOH. The control over the etching conditions can lead to various mesoporous morphologies useful in the drug delivery. PCPs can also serve as platforms to investigate the complex work of nature in virus construction and to unravel fundamental properties of these infecting bodies [217]. Polypeptide composite particles with magnetic inclusions are appealing. In addition to the magnetic response itself, which can alter rheological behavior through chaining, these particles can be recovered and, in some cases, reused. This helps to offset the complexity and expense of the synthetic procedures. In addition, collection of the particles is convenient during synthesis—for example to isolate the particles from catalysts or during solvent changes. Scheme 19 displays present and prospective applications of PCPs, including some non-covalent variants [207–212, 215].

The most likely application of PCPs is drug encapsulation and delivery. Void-shell morphologies aka capsules or vesicles have already been produced by layer-by-layer assembly of oppositely charged polypeptides, as described in “[Layer-by-layer assembly of oppositely charged polypeptides](#)” section. Future approaches will probably give attention to multi-compartment vesicles capable of selective payload release. Exposed to external stimuli such as change in pH, temperature, and solvent, polypeptides change their secondary conformation. This feature can be exploited to deliver pharmaceuticals. Two other applications of PCPs are jamming and self-assembly driven by various factors. The latter will be further developed during this section.

PCPs containing a magnetic core have found specific applications as gold supports in catalysis processes and as drug carriers. Marcelo et al. prepared magnetic particles coated with PBLG by ROP of BLG initiated by amino groups of dopamine-functionalized magnetite as shown in Scheme 20 [218].

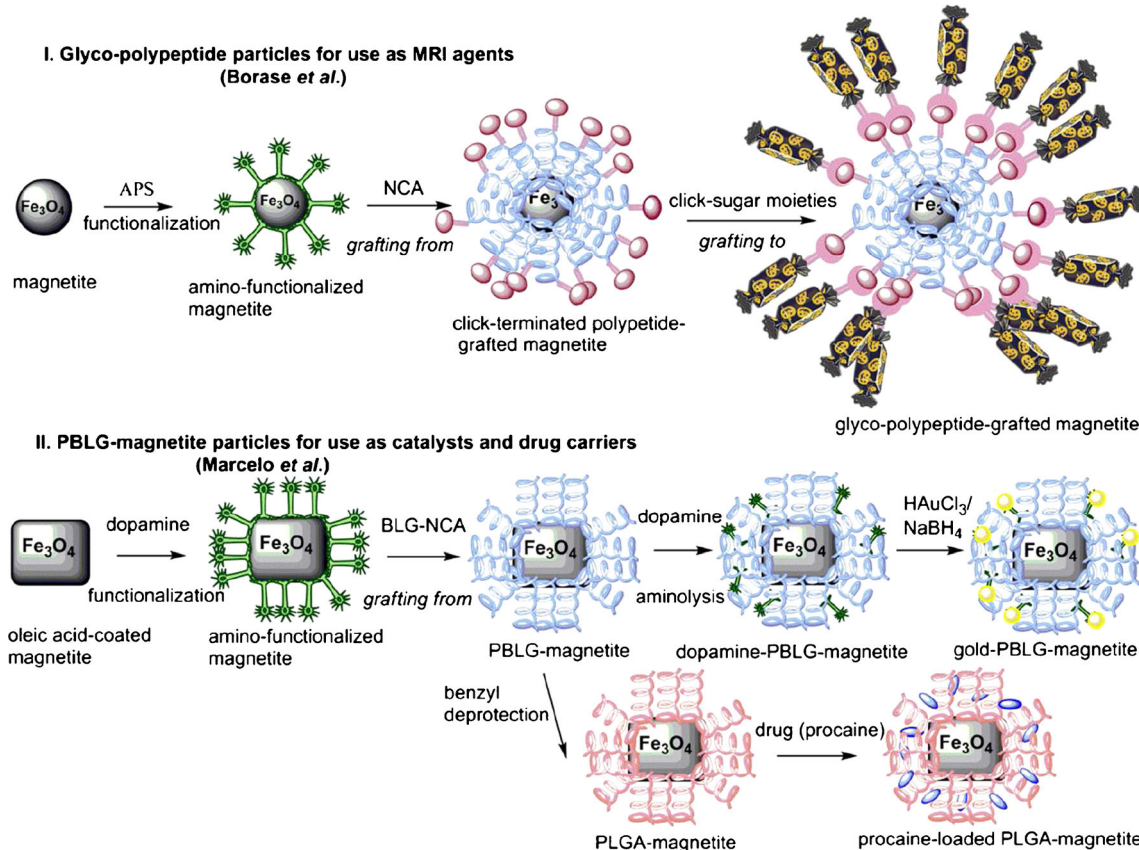
After partial exchange of benzyl substituents on the PBLG side chains with dopamine, the particles were able to attach colloidal gold. The catalytic efficiency of gold-primed PBLG magnetic particles was demonstrated by the reduction reaction of nitrophenol to aminophenol. After five cycles, the conversion began to decrease. After eight cycles, the reduction reaction proceeded for 24 h without reaching full conversion. Particles were easy to recover by magnetic separation but subsequent washings may have affected their catalytic activity. The control over the gold loading could also be another perturbing factor. Again, the grafting density plays an



Scheme 19 Present and prospective applications of PCPs

important role. The second dopamine loading to functionalize the shell may have led to a too-crowded environment and consequently it was difficult for the gold particles to penetrate the shell in-depth and reach the amino groups of dopamine. Marcelo et al. went a step further when they used PBLG-magnetite particles to incorporate the drug procaine [219]. The chemistry of drug incorporation was mediated by deprotection of PBLG side chains combined with carbodiimide (EDC/NHS) coupling and yielded water-soluble poly(L-glutamic) acid-based particles. Different polypeptide loadings were achieved and the saturation magnetization measurements indicated that the magnetic properties of the magnetite core were not affected. An approximate molecular weight evaluation of the shell was attempted by combining its thickness as observed by TEM with the PBLG helix parameters. The polymerization degree obtained was approximated as 105–120. Still, dry-down artifacts could affect the accurate visualization of the polypeptide shell in TEM.

PCPs with magnetic inclusions were envisioned as suitable MRI-trackable particles. Their efficiency was shadowed by the particle coalescence. Stable aqueous dispersions of magnetic nanoparticles were obtained by the combination of two types of chemistry: glycosylation and click giving rise to a new subclass of PCPs, glyco-polypeptide composite particles. Carbohydrate moieties promote colloidal stability through



Scheme 20 Illustration of glyco-polypeptide-grafted magnetite and gold/procaine-loaded polypeptide-magnetite preparation. See Borase et al. [220] and Marcelo et al. [218, 219]

charge and steric interactions. Borase et al. have used a two-step process using a combination of the *grafting from* method and Huisgen click reaction to obtain glycopeptide-grafted magnetic particles [220]. First, poly(L-glutamate) with clickable propargyl end-groups was grown from the particles surface by ROP of the corresponding NCA. Second, glycosylation was achieved by coupling propargyl-terminated polypeptide chains to azide-functionalized galactose through click chemistry. Even though the synthetic routes may be challenging, the alkyne-PLGA particles were found to be an efficient substrate to increase the surface density of functional monosaccharides. The monosaccharides were used to stabilize the magnetic dispersions against aggregation, a sensitive issue in using magnetic particles as efficient MRI contrast agents. Borase et al. demonstrated the first example of well-dispersed nanoparticles where the density of functional groups used to anchor the galactose units was not dependent on the nanoparticle surface area. The particles were designed for use as T1-weighting (localized signal enhancement) agents for magnetic resonance imaging (MRI). Another specific targeting was demonstrated by binding *Ricinus communis agglutinin* (RCA₂₀) lectin to the magnetic particles furnished with galactose units. Further investigations are extended to

other monosaccharide moieties and polymer chain length and follow their influence on MRI properties and cellular uptake.

Turning now to possible applications in polymer and colloid physics, PCPs offer a special opportunity to understand particle–polymer and particle–particle interactions because the softness of the shell can be varied using conformational transitions. The most studied materials, colloidal hard spheres, were shown to exhibit slow relaxation dynamics under crowded conditions as a result of either repulsive or attractive forces. Jammed soft matter evolves from a flowing to a rigid state as concentration is increased [221]. Even though the dynamics change dramatically, the internal structure remains disordered in both solid and fluid phase, quite different from crystallization [222]. Rheological behavior (see reference [223] for reviews) and the influence of external electromagnetic fields [224] on colloids are the main tools to understand jamming. The mutual interactions between particles suspended in a liquid are greatly influenced by the particulate size [225, 226] and does influence the stability of the suspension, either in a confined volume or flowing along a surface [227].

Core–shell particles confined in a polymer matrix were used as models to investigate self-assembly. When it comes

to probe diffusion measurements, any forthcoming PCP/polymer work should refer back to the milestone established by Tracy and Pecora on the ternary system silica/PBLG/DMF at different concentrations [228]. The diffusion coefficients of 60.4 nm hard spheres suspended in PBLG of 70 nm in length could be measured simultaneously and were found to deviate from the theoretical calculations. The deviation found in the rod and coil solutions suggested that the hydrodynamic interactions between the polymer chains play an important role. From the biological point of view and the applications that may arise, the study of ternary systems using particles coated with a homopolypeptide shell suspended in the same or different helical polypeptide matrix as the shell, as depicted in Scheme 19, is at the beginning. A recent report has used another system to investigate the complex interaction between mixture components [229]. Useful techniques recently emerging are devoted to offer high-resolution information on such advanced materials and their dynamics. Micro-rheology using optical tweezers is one of these methods, as reviewed by Svoboda and Block [230]. Forces acting on single colloids or polymer-grafted particles without any mechanical contact that can be carried out in nano- and microfluidics can be measured. Trapped in the focal point of the strongly focused lasers, a particle is held and manipulated in the desirable medium enabling excellent insight especially on the pair interaction, the electrophoretic mobility, and drag forces, respectively [231]. Attached to a magnetic bead with one end, they could investigate the behavior of the DNA strand under different conditions. The progress in the field over the past decades enables high-resolution experiments on single cell adhesion [232] or parasite entity manipulation [233].

One of the most extraordinary and unique features that polypeptides provide is their capability to undergo conformational changes as a function of pH, temperature, or solvent. Stimuli-responsive polymeric micelles, capsules, or polymersomes found a myriad of applications from cosmetics, pharmaceuticals, and biotechnology to biomedicine. Steps toward introducing polypeptide-coated silica as biodegradable and easy-to-manipulate platforms to the field of such applications were made and this area continues to grow. Borase et al. also entrapped Rhodamine B within PLGA composites which was released upon pH variation (2–10) [131]. The Rhodamine B release mechanism can be considered a good model for future pH-responsive payload delivery. Furthermore, the feasibility of the bioconjugation was demonstrated by the attachment of a green fluorescent protein using NHS coupling chemistry. Aggregate particles were visualized by using fluorescence microscopy. Kar et al. [189] explored the potential of the PLGA-based particles as a biodegradable platform in the preparation of the scaffolds for drug delivery, MRI contrast agents, and tissue engineering applications. Well-defined, aligned three-dimensional macroporous structures were

produced from PLGA-grafted silica particles crosslinked with polyethyleneimine (PEI) using an ice templating approach with directional freezing. The PEI treatment stabilized the scaffold against water disassembly. The presence of the PLGA makes possible the post-functionalization with other organic moieties for tissue engineering applications.

A different approach to PCP architecture was developed by the Lecommandoux group using vesicles. First, the shell was prepared by self-assembly of the polypeptide-containing diblocks followed by the encapsulation of cores as magnetic guides. These self-assembled structures resemble in their structure primitive biological cells. Sanson et al. synthesized biocompatible block copolymers from poly(trimethylene carbonate)-b-poly(L-glutamic acid) that formed vesicles, and their sizes and dispersities were controlled under different conditions (e.g., polymer concentration, nature of organic phase, etc.) [234, 235]. The polyelectrolytic PLGA corona responded to the pH changes. The encapsulation of superparamagnetic maghemite, $\gamma\text{-Fe}_2\text{O}_3$, within the membrane of the vesicles by a nanoprecipitation process enhanced their responsiveness; the vesicles could be guided by external magnetic fields [236]. Furthermore, by loading with an anti-tumor drug such as doxorubicin hydrochloride, their use as complex drug carriers and as potential candidates for controlled drug release by radio frequency magnetic hyperthermia was demonstrated [237].

It is difficult to control the self-assembly of polypeptides and block polypeptides into uniform capsids or vesicles. PCPs can be considered an alternate route to such morphologies. The well-controlled size of the silica coupled to the etching techniques allows the formation of the target product. In addition, an approach to increase the lifetime and stability of void soft shells is the crosslinking. The conformational changes have been also exploited when polypeptides such as PBLG were deposited on flat and porous surfaces such as silicon and anodic alumina [238]. The product, polypeptide nanoporous alumina hybrid waveguide, is a potential platform with a high density of functional sites for sensing and drug purification purposes. PCPs have a higher specific area compared to polypeptides on flat surfaces; therefore, in the future, PCPs can be used to prime the flat and nanoporous surfaces enabling a high load of polypeptide.

No matter the procedure involved in the preparation of polypeptide containers (whether called polymersomes, micelles, vesicles, capsids, or capsosomes), the future lies with more complex structures featuring enhanced responsiveness, biocompatibility, and multiple compartments. The potential for such advanced materials was already demonstrated, for example, by Caruso's capsosomes used as platforms to future therapeutic cells and organocells [214, 239]. These particles exemplify the potential future applications of hybrid particles, which range from biomedicine to simple cosmetics.

Acknowledgments The authors thank the National Science Foundation (Grant No 1005707 and Grant No 1306262) for financial support.

References

- Lettinga MP, van Zandvoort M, van Kats CM, Philipse AP (2000) Phosphorescent colloidal silica spheres as tracers for rotational diffusion studies. *Langmuir* 16(15):6156–6165. doi:[10.1021/la9916023](https://doi.org/10.1021/la9916023)
- Salgueirino-Maceira V, Correa-Duarte MA (2007) Increasing the complexity of magnetic core/shell structured nanocomposites for biological applications. *Adv Mater* 19(23):4131–4144. doi:[10.1002/adma.200700418](https://doi.org/10.1002/adma.200700418)
- Martel S, Tremblay CC, Ngakeng S, Langlois G (2006) Controlled manipulation and actuation of micro-objects with magnetotactic bacteria. *Appl Phys Lett* 89(23):233904
- Zou H, Wu SS, Shen J (2008) Polymer/silica nanocomposites: preparation, characterization, properties, and applications. *Chem Rev* 108(9):3893–3957. doi:[10.1021/cr068035q](https://doi.org/10.1021/cr068035q)
- Dietz E, Fery N, Hamann K (1974) Polyreactions on pigmented surfaces. 4. Polymerization of n-carboxy-alpha-amino-acid anhydrides on surface of silicon dioxide. *Angew Makromol Chem* 35: 115–129
- Heise A, Menzel H, Yim H, Foster MD, Wieringa RH, Schouten AJ, Erb V, Stamm M (1997) Grafting of polypeptides on solid substrates by initiation of N-carboxyanhydride polymerization by amino-terminated self-assembled monolayers. *Langmuir* 13(4): 723–728
- Tsubokawa N, Kobayashi K, Sone Y (1987) Grafting of polypeptide from carbon black by the ring-opening polymerization of γ -methyl L-glutamate N-carboxyanhydride initiated by amino groups on carbon black surface. *Polym J* 19(10):1147–1155
- Fong B, Russo PS (1999) Organophilic colloidal particles with a synthetic polypeptide coating. *Langmuir* 15(13):4421–4426. doi:[10.1021/la9815648](https://doi.org/10.1021/la9815648)
- Wang YL, Chang YC (2003) Synthesis and conformational transition of surface-tethered polypeptide: poly(L-glutamic acid). *Macromolecules* 36(17):6503–6510. doi:[10.1021/ma034092z](https://doi.org/10.1021/ma034092z)
- Block H (1983) Poly(γ -benzyl-L-glutamate) and other glutamic acid containing polymers. Gordon and Breach, New York
- Miller WG (1978) Stiff chain polymer lyotropic liquid-crystals. *Annu Rev Phys Chem* 29:519–535. doi:[10.1146/annurev.pc.29.100178.002511](https://doi.org/10.1146/annurev.pc.29.100178.002511)
- Hamley IW (2010) Liquid crystal phase formation by biopolymers. *Soft Matter* 6(9):1863–1871. doi:[10.1039/b923942a](https://doi.org/10.1039/b923942a)
- Yen CC, Taguchi Y, Tokita M, Watanabe J (2010) Spontaneous formation of polar liquid crystal in lyotropic solution of helical poly(γ -benzyl glutamate). *Mol Cryst Liq Cryst* 516:91–98. doi:[10.1080/15421400903400712](https://doi.org/10.1080/15421400903400712)
- Daly WH, Poché D, Negulescu II (1994) Poly ([γ -alkyl-[α]-L-glutamate)s, derived from long chain paraffinic alcohols. *Prog Polym Sci* 19(1):79–135
- Doty P, Yang JT (1956) Polypeptides. 7. Poly-gamma-benzyl-L-glutamate—the helix-coil transition in solution. *J Am Chem Soc* 78(2):498–500
- Blout ER, Lenormant H (1957) Reversible configurational changes in poly-L-lysine hydrochloride induced by water. *Nature* 179(4567):960–963. doi:[10.1038/179960a0](https://doi.org/10.1038/179960a0)
- Applequist J (1963) On helix-coil equilibrium in polypeptides. *J Chem Phys* 38(4):934. doi:[10.1063/1.1733787](https://doi.org/10.1063/1.1733787)
- Karasz FE, O'Reilly JM, Bair HE (1964) Thermal helix-coil transition in poly-gamma-benzyl-L-glutamate. *Nature* 202(493):693. doi:[10.1038/202693b0](https://doi.org/10.1038/202693b0)
- Watanabe H, Yoshioka K, Wada A (1964) Electrooptical and dielectric investigations on the conformation and the electrical properties of poly-gamma-benzyl-L-glutamate in mixed solvents. *Biopolymers* 2(1):91–101. doi:[10.1002/bip.1964.360020112](https://doi.org/10.1002/bip.1964.360020112)
- Ackerman T, Neumann E (1967) Experimental thermodynamics of helix-random coil transition. 1. Influence of polymer concentration and solvent composition in PBG-DCA-EDC system. *Biopolymers* 5(7):649. doi:[10.1002/bip.1967.360050706](https://doi.org/10.1002/bip.1967.360050706)
- Itoh T, Hatanaka T, Ihara E, Inoue K (2012) Helix-coil transformation of poly(gamma-benzyl-L-glutamate) with polystyrene attached to the N or C terminus in trifluoroacetic acid-chloroform mixtures. *Polym J* 44(2):189–194. doi:[10.1038/pj.2011.113](https://doi.org/10.1038/pj.2011.113)
- Wen KJ, Woody RW (1975) Conformational studies of poly(L-tyrosine)—helix-coil transition in dimethyl sulfoxide dichloroacetic acid mixtures. *Biopolymers* 14(9):1827–1840. doi:[10.1002/bip.1975.360140905](https://doi.org/10.1002/bip.1975.360140905)
- Omura I, Teramoto A, Fujita H (1975) Dielectric-dispersion of polypeptide solutions. 2. Helix-coil transition of “poly(epsilon-carbobenzoxy-L-lysine) in m-cresol”. *Macromolecules* 8(3):284–290
- Wada A (1971) Dielectric evidence of chemical relaxation in the helix-coil transition of polypeptides. *Chem Phys Lett* 8(2):211–213
- Huang J, Heise A (2013) Stimuli responsive synthetic polypeptides derived from N-carboxyanhydride (NCA) polymerisation. *Chem Soc Rev*. doi:[10.1039/c3cs60063g](https://doi.org/10.1039/c3cs60063g)
- Sakajiri K, Satoh K, Yen CC, Tokita M, Watanabe J (2011) Helix-helix transition of poly(beta-phenylpropyl L-aspartate) embedded in stable helical poly(gamma-phenylethyl glutamate) matrix. *Polymer* 52(22):5053–5057. doi:[10.1016/j.polymer.2011.09.008](https://doi.org/10.1016/j.polymer.2011.09.008)
- Sallach RE, Wei M, Biswas N, Conticello VP, LeCommandoux S, Dluhy RA, Chaikof EL (2006) Micelle density regulated by a reversible switch of protein secondary structure. *J Am Chem Soc* 128(36):12014–12019
- Iler RK (1955) Colloid chemistry of silica and silicates. Cornell University Press, Ithaca, New York
- Kolbe G (1956) The complex chemical behavior of silica. Jena, Germany
- Stober W, Fink A, Bohn E (1968) Controlled growth of monodisperse silica spheres in the micron size range. *J Colloid Interface Sci* 26:62–69
- Brinker CJS, Scherer GW (2004) Sol-gel science: the physics and chemistry of sol-gel processing. Academies Press, Boston
- Van Helden AK, Jansen JW, Vrij A (1981) Preparation and characterization of spherical monodisperse silica dispersions in nonaqueous solvents. *J Colloid Interface Sci* 81(2):354–368
- Bogush GH, Tracy MA, Zukoski CF (1988) Preparation of monodisperse silica particles—control of size and mass fraction. *J Non-Cryst Solids* 104(1):95–106. doi:[10.1016/0022-3093\(88\)90187-1](https://doi.org/10.1016/0022-3093(88)90187-1)
- Bogush GH, Zukoski CF (1991) Uniform silica particle-precipitation—an aggregative growth-model. *J Colloid Interface Sci* 142(1):19–34. doi:[10.1016/0021-9797\(91\)90030-c](https://doi.org/10.1016/0021-9797(91)90030-c)
- Matsoukas T, Gulari E (1991) Self-sharpening distributions revisited polydispersity in growth by monomer addition. *J Colloid Interface Sci* 145(2):557–562. doi:[10.1016/0021-9797\(91\)90385-1](https://doi.org/10.1016/0021-9797(91)90385-1)
- Zhang JH, Zhan P, Wang ZL, Zhang WY, Ming NB (2003) Preparation of monodisperse silica particles with controllable size and shape. *J Mater Res* 18(3):649–653
- Watanabe R, Yokoi T, Kobayashi E, Otsuka Y, Shimojima A, Okubo T, Tatsumi T (2011) Extension of size of monodisperse silica nanospheres and their well-ordered assembly. *J Colloid Interface Sci* 360(1):1–7. doi:[10.1016/j.jcis.2010.09.001](https://doi.org/10.1016/j.jcis.2010.09.001)
- Chang SM, Lee M, Kim W-S (2005) Preparation of large monodispersed spherical silica particles using seed particle growth. *J Colloid Interface Sci* 286(2):536–542
- Rao KS, El-Hami K, Kodaki T, Matsushige K, Makino K (2005) A novel method for synthesis of silica nanoparticles. *J Colloid Interface Sci* 289(1):125–131

40. Balamurugan M, Saravanan S (2012) Producing nanosilica from *Sorghum vulgare* seed heads. Powder Technol 224:345–350. doi:[10.1016/j.powtec.2012.03.017](https://doi.org/10.1016/j.powtec.2012.03.017)
41. Sugimoto M (1999) The past, present, and future of ferrites. J Am Ceram Soc 82(2):269–280
42. Rado GT, Suhl H (1963) Magnetism VIII: spin arrangements and crystal structure, domains, and micromagnetics. Academic Press Inc, London
43. Khalafalla SE, Reimers GW (1980) Preparation of dilution-stable aqueous magnetic fluids. IEEE Trans Magn 16(2):178–183. doi:[10.1109/tmag.1980.1060578](https://doi.org/10.1109/tmag.1980.1060578)
44. Massart R (1981) Preparation of aqueous magnetic liquids in alkaline and acidic media. IEEE Trans Magn 17(2):1247–1248. doi:[10.1109/tmag.1981.1061188](https://doi.org/10.1109/tmag.1981.1061188)
45. Philipse AP, Vanbruggen MPB, Pathmamanoharan C (1994) Magnetic silica dispersions—preparation and stability of surface-modified silica particles with a magnetic core. Langmuir 10(1):92–99. doi:[10.1021/la00013a014](https://doi.org/10.1021/la00013a014)
46. van Ewijk GA, Vroege GJ, Philipse AP (1999) Convenient preparation methods for magnetic colloids. J Magn Magn Mater 201:31–33. doi:[10.1016/s03048853\(99\)00080-3](https://doi.org/10.1016/s03048853(99)00080-3)
47. Wang H, Nakamura H, Yao K, Maeda H, Abe E (2001) Effect of solvents on the preparation of silica-coated magnetic particles. Chem Lett 11:1168–1169
48. Aliev FG, Correa-Duarte MA, Mamedov A, Ostrander JW, Giersig M, Liz-Marzan LM, Kotov NA (1999) Layer-by-layer assembly of core-shell magnetite nanoparticles: effect of silica coating on interparticle interactions and magnetic properties. Adv Mater 11(12): 1006–1010. doi:[10.1002/\(sici\)15214095\(199908\)11:12<1006::aid-adma1006>3.0.co;2-2](https://doi.org/10.1002/(sici)15214095(199908)11:12<1006::aid-adma1006>3.0.co;2-2)
49. Bruce IJ, Taylor J, Todd M, Davies MJ, Borioni E, Sangregorio C, Sen T (2004) Synthesis, characterisation and application of silica-magnetite nanocomposites. J Magn Magn Mater 284:145–160. doi:[10.1016/j.jmmm.2004.06.032](https://doi.org/10.1016/j.jmmm.2004.06.032)
50. Lu Y, Yin YD, Mayers BT, Xia YN (2002) Modifying the surface properties of superparamagnetic iron oxide nanoparticles through a sol–gel approach. Nano Lett 2(3):183–186. doi:[10.1021/nl015681q](https://doi.org/10.1021/nl015681q)
51. Tsai YL, Chun CH, Ou JL, Huang CK, Chen CC (2006) Magnetic Fe₃O₄ nanoparticles synthesized for preparations of silica-coated composites. Desalination 200(1–3):97–99. doi:[10.1016/j.desal.2006.03.256](https://doi.org/10.1016/j.desal.2006.03.256)
52. Yang D, Hu JH, Fu SK (2009) Controlled synthesis of magnetite-silica nanocomposites via a seeded sol–gel approach. J Phys Chem C 113(18):7646–7651. doi:[10.1021/jp900868d](https://doi.org/10.1021/jp900868d)
53. Iida H, Takayanagi K, Nakanishi T, Osaka T (2007) Synthesis of Fe₃O₄ nanoparticles with various sizes and magnetic properties by controlled hydrolysis. J Colloid Interface Sci 314(1):274–280. doi:[10.1016/j.jcis.2007.05.047](https://doi.org/10.1016/j.jcis.2007.05.047)
54. Colombo M, Carregal-Romero S, Casula MF, Gutierrez L, Morales MP, Bohm IB, Heverhagen JT, Prosperi D, Parak WJ (2012) Biological applications of magnetic nanoparticles. Chem Soc Rev 41(11):4306–4334
55. Faraji M, Yamini Y, Rezaee M (2010) Magnetic nanoparticles: synthesis, stabilization, functionalization, characterization, and applications. J Iran Chem Soc 7(1):1–37
56. Shen LF, Laibinis PE, Hatton TA (1999) Bilayer surfactant stabilized magnetic fluids: synthesis and interactions at interfaces. Langmuir 15(2):447–453. doi:[10.1021/la9807661](https://doi.org/10.1021/la9807661)
57. Hong RY, Li JH, Li HZ, Ding J, Zheng Y, Wei DG (2008) Synthesis of Fe₃O₄ nanoparticles without inert gas protection used as precursors of magnetic fluids. J Magn Magn Mater 320(9):1605–1614. doi:[10.1016/j.jmmm.2008.01.015](https://doi.org/10.1016/j.jmmm.2008.01.015)
58. Liu ZL, Wang HB, Lu QH, Du GH, Peng L, Du YQ, Zhang SM, Yao KL (2004) Synthesis and characterization of ultrafine well-dispersed magnetic nanoparticles. J Magn Magn Mater 283(2–3): 258–262. doi:[10.1016/j.jmmm.2004.05.031](https://doi.org/10.1016/j.jmmm.2004.05.031)
59. Kim DK, Zhang Y, Voit W, Rao KV, Muhammed M (2001) Synthesis and characterization of surfactant-coated superparamagnetic monodispersed iron oxide nanoparticles. J Magn Magn Mater 225(1–2):30–36. doi:[10.1016/s03048853\(00\)01224-5](https://doi.org/10.1016/s03048853(00)01224-5)
60. Chaudhuri RG, Paria S (2012) Core/shell nanoparticles: classes, properties, synthesis mechanisms, characterization, and applications. Chem Rev 112(4):2373–2433. doi:[10.1021/cr100449n](https://doi.org/10.1021/cr100449n)
61. Willard MA, Kurihara LK, Carpenter EE, Calvin S, Harris VG (2004) Chemically prepared magnetic nanoparticles. Int Mater Rev 49(3–4):125–170. doi:[10.1179/095066004225021882](https://doi.org/10.1179/095066004225021882)
62. Ban I, Drofenik M, Makovec D (2005) The synthesis of silica-coated permalloy nanoparticles using a water-in-oil microemulsion. In: Uskokovic DP, Milonjic SK, Rakovic DI (eds) Current Research in Advanced Materials and Processes, 494, pp 161–165
63. Liu YM, Wu YC (2012) Synthesis of europium-doped silica microspheres using the sol–gel microencapsulation method. J Sol–gel Sci Technol 63(1):36–44. doi:[10.1007/s10971-012-2760-4](https://doi.org/10.1007/s10971-012-2760-4)
64. Lin JC, Dipre JT, Yates MZ (2003) Microemulsion-directed synthesis of molecular sieve fibers. Chem Mat 15(14):2764–2773. doi:[10.1021/cm0341437](https://doi.org/10.1021/cm0341437)
65. Shchukin DG, Sukhorukov GB (2004) Nanoparticle synthesis in engineered organic nanoscale reactors. Adv Mater 16(8):671–682. doi:[10.1002/adma.200306466](https://doi.org/10.1002/adma.200306466)
66. Saito T, Ohshima S, Xu WC, Ago H, Yumura M, Iijima S (2005) Size control of metal nanoparticle catalysts for the gas-phase synthesis of single-walled carbon nanotubes. J Phys Chem B 109(21): 10647–10652. doi:[10.1021/jp044200z](https://doi.org/10.1021/jp044200z)
67. Shangguan T, Cabral-Lilly D, Purandare U, Godin N, Ahl P, Janoff A, Meers P (2000) A novel N-acyl phosphatidylethanolamine-containing delivery vehicle for spermine-condensed plasmid DNA. Gene Ther 7(9):769–783. doi:[10.1038/sj.gt.3301156](https://doi.org/10.1038/sj.gt.3301156)
68. Pileni MP (2001) Nanocrystal self-assemblies: fabrication and collective properties. J Phys Chem B 105(17):3358–3371. doi:[10.1021/jp0039520](https://doi.org/10.1021/jp0039520)
69. Asua JM (2002) Miniemulsion polymerization. Prog Polym Sci 27(7):1283–1346
70. Uskokovic V, Drofenik M (2005) Synthesis of materials within reverse micelles. Surf Rev Lett 12(2):239–277. doi:[10.1142/s0218625x05007001](https://doi.org/10.1142/s0218625x05007001)
71. Dinega DP, Bawendi MG (1999) A solution-phase chemical approach to a new crystal structure of cobalt. Angew Chem Int Edit 38(12):1788–1791. doi:[10.1002/\(sici\)1521-3773\(19990614\)38:12<1788::aid-anie1788>3.0.co;2-2](https://doi.org/10.1002/(sici)1521-3773(19990614)38:12<1788::aid-anie1788>3.0.co;2-2)
72. Tracy JB, Weiss DN, Dinega DP, Bawendi MG (2005) Exchange biasing and magnetic properties of partially and fully oxidized colloidal cobalt nanoparticles. Physical Review B 72(6): 064404. doi:[10.1103/PhysRevB.72.064404](https://doi.org/10.1103/PhysRevB.72.064404)
73. Hess PH, Parker PH (1966) Polymers for stabilization of colloidal cobalt particles. J Appl Polym Sci 10(12):1915. doi:[10.1002/app.1966.070101209](https://doi.org/10.1002/app.1966.070101209)
74. Ould-Ely T, Amiens C, Chaudret B, Snoeck E, Verelst M, Respaud M, Broto JM (1999) Synthesis of nickel nanoparticles. Influence of aggregation induced by modification of poly(vinylpyrrolidone) chain length on their magnetic properties. Chem Mat 11(3):526
75. Carpenter EE, Sangregorio C, O'Connor CJ (1999) Effects of shell thickness on blocking temperature of nanocomposites of metal particles with gold shells. IEEE Trans Magn 35(5):3496–3498. doi:[10.1109/20.800568](https://doi.org/10.1109/20.800568)
76. Sobal NS, Hilgendorff M, Mohwald H, Giersig M, Spasova M, Radetic T, Farle M (2002) Synthesis and structure of colloidal bimetallic nanocrystals: the non-alloying system Ag/Co. Nano Lett 2(6):621–624. doi:[10.1021/nl025533f](https://doi.org/10.1021/nl025533f)
77. Nikitenko SI, Koltypin Y, Palchik O, Felner I, Xu XN, Gedanken A (2001) Synthesis of highly magnetic, air-stable iron carbide nanocrystalline particles by using power ultrasound. Angew Chem

- Int Edit 40(23):4447. doi:[10.1002/15213773\(20011203\)40:23<4447::aid-anie4447>3.0.co;2-j](https://doi.org/10.1002/15213773(20011203)40:23<4447::aid-anie4447>3.0.co;2-j)
78. Liz-Marzan LM, Giersig M, Mulvaney P (1996) Homogeneous silica coating of vitreophobic colloids. *Chem Commun* 6:731–732. doi:[10.1039/cc9960000731](https://doi.org/10.1039/cc9960000731)
 79. Kobayashi Y, Horie M, Konno M, Rodriguez-Gonzalez B, Liz-Marzan LM (2003) Preparation and properties of silica-coated cobalt nanoparticles. *J Phys Chem B* 107(30):7420–7425. doi:[10.1021/jp027759c](https://doi.org/10.1021/jp027759c)
 80. Guerrero-Martinez A, Perez-Juste J, Liz-Marzan LM (2010) Recent progress on silica coating of nanoparticles and related nanomaterials. *Adv Mater* 22(11):1182–1195. doi:[10.1002/adma.200901263](https://doi.org/10.1002/adma.200901263)
 81. Repko A, Niznansky D, Poltierova-Vejpravova J (2011) A study of oleic acid-based hydrothermal preparation of CoFe_2O_4 nanoparticles. *J Nanopart Res* 13(10):5021–5031. doi:[10.1007/s11051-011-0483-z](https://doi.org/10.1007/s11051-011-0483-z)
 82. Sun SH, Zeng H, Robinson DB, Raoux S, Rice PM, Wang SX, Li GX (2004) Monodisperse MFe_2O_4 ($\text{M}=\text{Fe}, \text{Co}, \text{Mn}$) nanoparticles. *J Am Chem Soc* 126(1):273–279. doi:[10.1021/ja0380852](https://doi.org/10.1021/ja0380852)
 83. Kwon SG, Piao Y, Park J, Angappane S, Jo Y, Hwang NM, Park JG, Hyeon T (2007) Kinetics of monodisperse iron oxide nanocrystal formation by “heating-up” process. *J Am Chem Soc* 129(41):12571–12584. doi:[10.1021/ja074633q](https://doi.org/10.1021/ja074633q)
 84. Roca AG, Morales MP, O’Grady K, Serna CJ (2006) Structural and magnetic properties of uniform magnetite nanoparticles prepared by high temperature decomposition of organic precursors. *Nanotechnology* 17(11):2783–2788. doi:[10.1088/0957-4484/17/11/010](https://doi.org/10.1088/0957-4484/17/11/010)
 85. Ravikumar C, Bandyopadhyaya R (2011) Mechanistic study on magnetite nanoparticle formation by thermal decomposition and coprecipitation routes. *J Phys Chem C* 115(5):1380–1387. doi:[10.1021/jp105304w](https://doi.org/10.1021/jp105304w)
 86. Wu S, Sun AZ, Zhai FQ, Wang J, Xu WH, Zhang Q, Volinsky AA (2011) Fe_3O_4 magnetic nanoparticles synthesis from tailings by ultrasonic chemical co-precipitation. *Mater Lett* 65(12):1882–1884. doi:[10.1016/j.matlet.2011.03.065](https://doi.org/10.1016/j.matlet.2011.03.065)
 87. Zhang SJ, Liu XH, Zhou LP, Peng WJ (2012) Magnetite nanostructures: one-pot synthesis, superparamagnetic property and application in magnetic resonance imaging. *Mater Lett* 68:243–246. doi:[10.1016/j.matlet.2011.10.070](https://doi.org/10.1016/j.matlet.2011.10.070)
 88. Mizutani N, Iwasaki T, Watano S, Yanagida T, Kawai T (2010) Size control of magnetite nanoparticles in hydrothermal synthesis by coexistence of lactate and sulfate ions. *Curr Appl Phys* 10(3):801–806. doi:[10.1016/j.cap.2009.09.018](https://doi.org/10.1016/j.cap.2009.09.018)
 89. Xu CB, Teja AS (2008) Continuous hydrothermal synthesis of iron oxide and PVA-protected iron oxide nanoparticles. *J Supercrit Fluids* 44(1):85–91. doi:[10.1016/j.supflu.2007.09.033](https://doi.org/10.1016/j.supflu.2007.09.033)
 90. Hou YL, Kondoh H, Shimojo M, Kogure T, Ohta T (2005) High-yield preparation of uniform cobalt hydroxide and oxide nanoplatelets and their characterization. *J Phys Chem B* 109(41):19094–19098. doi:[10.1021/jp0521149](https://doi.org/10.1021/jp0521149)
 91. You-Ping Y, Ren-Sheng L, Ke-Long H, Li-Ping W, Su-Qin L, Wen-Wen Z (2007) Preparation and electrochemical performance of nanosized Co_3O_4 via hydrothermal method. *T Nonferr Metal Soc* 17(6):1334–1338
 92. Cannas C, Musinu A, Ardu A, Orru F, Peddis D, Casu M, Sanna R, Angius F, Diaz G, Piccaluga G (2010) CoFe_2O_4 and $\text{CoFe}_2\text{O}_4/\text{SiO}_2$ core/shell nanoparticles: magnetic and spectroscopic study. *Chem Mat* 22(11):3353–3361. doi:[10.1021/cm903837g](https://doi.org/10.1021/cm903837g)
 93. Komarneni S, Katsuki H (2002) Nanophase materials by a novel microwave-hydrothermal process. *Pure Appl Chem* 74(9):1537–1543. doi:[10.1351/pac200274091537](https://doi.org/10.1351/pac200274091537)
 94. Balasubramaniam C, Khollam YB, Bannerjee I, Bakare PP, Date SK, Das AK, Bhoraskar S (2004) DC thermal arc-plasma preparation of nanometric and stoichiometric spherical magnetite (Fe_3O_4) powders. *Mater Lett* 58(30):3958–3962. doi:[10.1016/j.matlet.2004.09.003](https://doi.org/10.1016/j.matlet.2004.09.003)
 95. Kim KM, Kang JH, Vinu A, Choy JH, Oh JM (2013) Inorganic nanomedicines and their labeling for biological imaging. *Curr Top Med Chem* 13(4):488–503
 96. Cintenza, L. O. (2010) Quantum dots in biomedical applications: advances and challenges. *J. Nanophotonics* 4(1):042503. doi:[10.42503/10.1117/1.3500388](https://doi.org/10.42503/10.1117/1.3500388)
 97. Salgueirino-Maceira V, Correa-Duarte MA, Spasova M, Liz-Marzan LM, Farle M (2006) Composite silica spheres with magnetic and luminescent functionalities. *Adv Funct Mater* 16(4):509–514. doi:[10.1002/adfm.200500565](https://doi.org/10.1002/adfm.200500565)
 98. Vanblaaderen A, Vrij A (1992) Synthesis and characterization of colloidal dispersions of fluorescent, monodisperse silica spheres. *Langmuir* 8(12):2921–2931. doi:[10.1021/la00048a013](https://doi.org/10.1021/la00048a013)
 99. Wang L, Tan WH (2006) Multicolor FRET silica nanoparticles by single wavelength excitation. *Nano Lett* 6(1):84–88. doi:[10.1021/nl052105b](https://doi.org/10.1021/nl052105b)
 100. Yang W, Zhang CG, Qu HY, Yang HH, Xu JG (2004) Novel fluorescent silica nanoparticle probe for ultrasensitive immunoassays. *Anal Chim Acta* 503(2):163–169. doi:[10.1016/j.aca.2003.10.045](https://doi.org/10.1016/j.aca.2003.10.045)
 101. Deng YH, Wang CC, Hu JH, Yang WL, Fu SK (2005) Investigation of formation of silica-coated magnetite nanoparticles via sol-gel approach. *Colloid Surf A* 262(1–3):87–93. doi:[10.1016/j.colsurfa.2005.04.009](https://doi.org/10.1016/j.colsurfa.2005.04.009)
 102. Giaume D, Poggi M, Casanova D, Mialon G, Lahilil K, Alexandrou A, Gacoin T, Boilot JP (2008) Organic functionalization of luminescent oxide nanoparticles toward their application as biological probes. *Langmuir* 24(19):11018–11026. doi:[10.1021/la8015468](https://doi.org/10.1021/la8015468)
 103. Vroman L (1974) Surface charge, protein adsorption, and thrombosis. *Science* 184(4136):585–586. doi:[10.1126/science.184.4136.585](https://doi.org/10.1126/science.184.4136.585)
 104. Sen T, Sebastianelli A, Bruce IJ (2006) Mesoporous silica-magnetite nanocomposite: fabrication and applications in magnetic bioseparations. *J Am Chem Soc* 128(22):7130–7131. doi:[10.1021/ja061393q](https://doi.org/10.1021/ja061393q)
 105. Deng Y, Qi D, Deng C, Zhang X, Zhao D (2008) Superparamagnetic high-magnetization microspheres with an $\text{Fe}_3\text{O}_4@\text{SiO}_2$ core and perpendicularly aligned mesoporous SiO_2 shell for removal of microcystins. *J Am Chem Soc* 130(1):28–+. doi:[10.1021/ja0777584](https://doi.org/10.1021/ja0777584)
 106. Coskun M, Korkmaz M, Firat T, Jaffari GH, Shah SI (2010) Synthesis of SiO_2 coated NiFe_2O_4 nanoparticles and the effect of SiO_2 shell thickness on the magnetic properties. *J. Appl. Phys.*, 107(9)
 107. Erathodiyil N, Ying JY (2011) Functionalization of inorganic nanoparticles for bioimaging applications. *Accounts Chem Res* 44(10):925–935. doi:[10.1021/ar2000327](https://doi.org/10.1021/ar2000327)
 108. Lallana E, Sousa-Herves A, Fernandez-Trillo F, Riguera R, Fernandez-Megia E (2012) Click chemistry for drug delivery nanosystems. *Pharm Res* 29(1):1–34. doi:[10.1007/s11095-011-0568-5](https://doi.org/10.1007/s11095-011-0568-5)
 109. Schladt TD, Schneider K, Schild H, Tremel W (2011) Synthesis and bio-functionalization of magnetic nanoparticles for medical diagnosis and treatment. *Dalton Trans* 40(24):6315–6343. doi:[10.1039/c0dt00689k](https://doi.org/10.1039/c0dt00689k)
 110. Wu W, He QG, Jiang CZ (2008) Magnetic iron oxide nanoparticles: synthesis and surface functionalization strategies. *Nanoscale Res Lett* 3(11):397–415. doi:[10.1007/s11671-008-9174-9](https://doi.org/10.1007/s11671-008-9174-9)
 111. Soto-Cantu E, Cueto R, Koch J, Russo PS (2012) Synthesis and rapid characterization of amine-functionalized silica. *Langmuir* 28(13):5562–5569. doi:[10.1021/la204981b](https://doi.org/10.1021/la204981b)
 112. Quang DV, Sarawade PB, Hilonga A, Kim JK, Chai YG, Kim SH, Ryu JY, Kim HT (2011) Preparation of amino functionalized silica micro beads by dry method for supporting silver nanoparticles with antibacterial properties. *Colloids Surf A* 389(1–3):118–126. doi:[10.1016/j.colsurfa.2011.08.042](https://doi.org/10.1016/j.colsurfa.2011.08.042)

113. Assink RA, Kay BD (1988) Sol-gel kinetics I. Functional group kinetics. *J Non-Cryst Solids* 99(2–31):359–370
114. Rother D, Sen T, East D, Bruce IJ (2011) Silicon, silica and its surface patterning/activation with alkoxy- and amino-silanes for nanomedical applications. *Nanomedicine* 6(2):281–300. doi:[10.2217/nnm.10.159](https://doi.org/10.2217/nnm.10.159)
115. Acosta EJ, Carr CS, Simanek EE, Shantz DF (2004) Engineering nanospaces: iterative synthesis of melamine-based dendrimers on amine-functionalized SBA-15 leading to complex hybrids with controllable chemistry and porosity. *Adv Mater* 16(12):985. doi:[10.1002/adma.200306323](https://doi.org/10.1002/adma.200306323)
116. Luechinger M, Prins R, Pirngruber GD (2005) Functionalization of silica surfaces with mixtures of 3-aminopropyl and methyl groups. *Microporous Mesoporous Mater* 85(1–2):111–118. doi:[10.1016/j.micromeso.2005.05.031](https://doi.org/10.1016/j.micromeso.2005.05.031)
117. Beck JS, Vartuli JC, Roth WJ, Leonowicz ME, Kresge CT, Schmitt KD, Chu CTW, Olson DH, Sheppard EW, McCullen SB, Higgins JB, Schlenker JL (1992) A new family of mesoporous molecular-sieves prepared with liquid-crystal templates. *J Am Chem Soc* 114(27):10834–10843. doi:[10.1021/ja00053a020](https://doi.org/10.1021/ja00053a020)
118. Burkett SL, Sims SD, Mann S (1996) Synthesis of hybrid inorganic–organic mesoporous silica by co-condensation of siloxane and organosiloxane precursors. *Chem Commun* 11:1367–1368. doi:[10.1039/cc9960001367](https://doi.org/10.1039/cc9960001367)
119. Wulff G, Heide B, Helfmeier G (1987) Enzyme-analog built polymers. 24. On the distance accuracy of functional-groups in polymers and silicas introduced by a template approach. *React Polym* 6(2–3):299–310
120. Bass JD, Katz A (2003) Thermolytic synthesis of imprinted amines in bulk silica. *Chem Mat* 15(14):2757–2763. doi:[10.1021/cm021822t](https://doi.org/10.1021/cm021822t)
121. McKittrick MW, Jones CW (2003) Toward single-site functional materials-preparation of amine-functionalized surfaces exhibiting site-isolated behavior. *Chem Mat* 15(5):1132–1139. doi:[10.1021/cm020952z](https://doi.org/10.1021/cm020952z)
122. McKittrick MW, Jones CW (2005) Modulating the reactivity of an organometallic catalyst via immobilization on a spatially patterned silica surface. *Chem Mat* 17(19):4758–4761. doi:[10.1021/cm050925j](https://doi.org/10.1021/cm050925j)
123. Khosroshahi ME, Ghazanfari L (2012) Synthesis and functionalization of SiO₂ coated Fe₃O₄ nanoparticles with amine groups based on self-assembly. *Mater Sci Eng C* 32(5):1043–1049. doi:[10.1016/j.msec.2011.09.003](https://doi.org/10.1016/j.msec.2011.09.003)
124. Xing YJ, Borguet E (2007) Specificity and sensitivity of fluorescence labeling of surface species. *Langmuir* 23(2):684–688. doi:[10.1021/la060994s](https://doi.org/10.1021/la060994s)
125. Aflori M, Drobotu M, Timpu D, Barboiu V (2008) Studies of amine treatments influence on poly(ethyleneterephthalate) films. *Optoelectron Adv Mat* 2(5):291–295
126. Kaiser E, Colescot R, Bossinge C, Cook PI (1970) Color test for detection of free terminal amino groups in solid-phase synthesis of peptides. *Anal Chem* 34(2):595. doi:[10.1016/0003-2697\(70\)90146-6](https://doi.org/10.1016/0003-2697(70)90146-6)
127. Coussot G, Faye C, Ibrahim A, Ramonda M, Dobrijevic M, Le Postollec A, Granier F, Vandenebelle-Trambouze O (2011) Aminated dendritic surfaces characterization: a rapid and versatile colorimetric assay for estimating the amine density and coating stability. *Anal Bioanal Chem* 399(6):2295–2302. doi:[10.1007/s00216-010-4612-9](https://doi.org/10.1007/s00216-010-4612-9)
128. Noel S, Liberelle B, Robitaille L, De Crescenzo G (2011) Quantification of primary amine groups available for subsequent biofunctionalization of polymer surfaces. *Bioconjugate Chem* 22(8):1690–1699. doi:[10.1021/bc200259c](https://doi.org/10.1021/bc200259c)
129. Chen Y, Zhang YQ (2011) Fluorescent quantification of amino groups on silica nanoparticle surfaces. *Anal Bioanal Chem* 399(7):2503–2509. doi:[10.1007/s00216-010-4622-7](https://doi.org/10.1007/s00216-010-4622-7)
130. Bartholome C, Beyou E, Bourgeat-Lami E, Chaumont P, Lefebvre F, Zydowicz N (2005) Nitroxide-mediated polymerization of styrene initiated from the surface of silica nanoparticles. In situ generation and grafting of alkoxyamine initiators. *Macromolecules* 38(4):1099–1106. doi:[10.1021/ma048501i](https://doi.org/10.1021/ma048501i)
131. Borase T, Iacono M, Ali SI, Thornton PD, Heise A (2012) Polypeptide core–shell silica nanoparticles with high grafting density by N-carboxyanhydride (NCA) ring opening polymerization as responsive materials and for bioconjugation. *Polym Chem* 3(5):1267–1275. doi:[10.1039/c2py00610c](https://doi.org/10.1039/c2py00610c)
132. Kricheldorf HR (1990) Models of biopolymers by ring-opening polymerization. CRC, Boca Raton, FL
133. Leuchs H, Geiger W (1908) Concerning the anhydride on alpha-amino-N-carbonic acids and that of alpha-amino acids. *Berichte Der Deutschen Chemischen Gesellschaft* 41:1721–1726. doi:[10.1002/cber.19080410232](https://doi.org/10.1002/cber.19080410232)
134. Curtius T (1930) The formation of urea from azide from mono- and dialkyl acetic acid. *J Fur Praktische Chemie Leipzig* 125(1/12):152–156. doi:[10.1002/prac.19301250109](https://doi.org/10.1002/prac.19301250109)
135. Wessely F, Sigmund F (1926) Investigations on alpha-amino-N-carbonic acid anhydrides. III. (On knowledge of highly molecular compounds). *Hoppe-Seylers Zeitschrift Fur Physiologische Chemie* 159(1/4):102–119. doi:[10.1515/bchm2.1926.159.1-4.102](https://doi.org/10.1515/bchm2.1926.159.1-4.102)
136. Fuchs F (1922) On N-carbonic acid-anhydride. *Berichte Der Deutschen Chemischen Gesellschaft* 55:2943–2943. doi:[10.1002/cber.19220550902](https://doi.org/10.1002/cber.19220550902)
137. Farthing AC, Reynolds RJW (1950) Anhydro-N-carboxy-DL-beta-phenylalanine. *Nature* 165(4199):647–647. doi:[10.1038/165647a0](https://doi.org/10.1038/165647a0)
138. Fuller WD, Verlander MS, Goodman M (1976) Procedure for facile synthesis of amino-acid n-carboxyanhydrides. *Biopolymers* 15(9):1869–1871. doi:[10.1002/bip.1976.360150922](https://doi.org/10.1002/bip.1976.360150922)
139. Cornille F, Copier J-L, Senet J-P, Robin Y (2002) Isochem Paris Cedex US Patent 6479665, 12 Nov 2002
140. Dorman LC, Shiang WR, Meyers PA (1992) Purification of gamma-benzyl and gamma-methyl L-glutamate N-carboxyanhydrides by rephosgenation. *Synth Commun* 22(22):3257–3262. doi:[10.1080/00397919208021140](https://doi.org/10.1080/00397919208021140)
141. Daly WH, Poché D (1988) The preparation of N-carboxyanhydrides of α -amino acids using bis(trichloromethyl)carbonate. *Tetrahedron Lett* 29(46):5859–5862
142. Wilder R, Mabashery S (1992) The use of triphosgene in preparation of N-carboxy-alpha-amino acid anhydrides. *J Org Chem* 57(9):2755–2756. doi:[10.1021/jo00035a044](https://doi.org/10.1021/jo00035a044)
143. Poché DS, Moore MJ, Bowles JL (1999) An unconventional method for purifying the N-carboxyanhydride derivatives of gamma-alkyl-L-glutamates. *Synth Commun* 29(5):843–854. doi:[10.1080/00397919908086042](https://doi.org/10.1080/00397919908086042)
144. Szwarc M (1965) The kinetics and mechanism of N-carboxy- α -amino-acid anhydride (NCA) polymerisation to poly-amino acids. *Advance in Polymer Science* 4:1–65
145. Dewey RS, Schoenew E, Joshua H, Paleveda WJ, Schwam H, Barkemey H, Arison BH, Veber DF, Strachan RG, Milkowsk J, Denkewal R, Hirschma R (1971) Synthesis of peptides in aqueous medium. 7. Preparation and use of 2,5-thiazolidinediones in peptide synthesis. *J Org Chem* 36(1):49
146. Kricheldorf HR (2006) Polypeptides and 100 years of chemistry of alpha-amino acid N-carboxyanhydrides. *Angew Chem Int Ed* 45(35):5752–5784. doi:[10.1002/anie.200600693](https://doi.org/10.1002/anie.200600693)
147. Voet D, Voet JG (1995). Wiley, New York
148. Kricheldorf HR (1977) Mechanism of NCA-polymerization. 4. Synthesis and reactions of N-acyl-NCA. *Macromol Chem Phys* 178(4):905–939
149. Waley SG, Watson J (1949) The kinetics of the polymerization of sarcosine carbonic anhydride. *Proc R Soc A* 199(1059):499–517. doi:[10.1098/rspa.1949.0151](https://doi.org/10.1098/rspa.1949.0151)
150. Lundberg RD, Doty P (1957) Polypeptides. 17. A study of the kinetics of the primary amine-initiated polymerization of N-

- carboxy-anhydrides with special reference to configurational and stereochemical effects. *J Am Chem Soc* 79(15):3961–3972
151. Frankel M, Katchalski E (1943) Derivatives of N-carboxy-alpha-amino acid esters. *J Am Chem Soc* 65:1670–1674. doi:[10.1021/ja01249a003](https://doi.org/10.1021/ja01249a003)
152. Heyns K, Schultze H, Brockmann R (1958) Zum mechanismus der polymerisation von aminosaure-N-carbonsaureanhydriden - untersuchungen zum isotopie-effekt.2. *Annalen Der Chemie-Justus Liebig* 611(1–3):33–39
153. Ballard DGH, Bamford CH (1954) Studies in polymerization. 7. The polymerization of N-carboxy-alpha-amino acid anhydrides. *Proc R Soc A* 223(1155):495–520. doi:[10.1098/rspa.1954.0133](https://doi.org/10.1098/rspa.1954.0133)
154. Kricheldorf HR, Von Lossow C, Schwarz G (2006) Tertiary amine catalyzed polymerizations of alpha-amino acid N-carboxyanhydrides: the role of cyclization. *J Polymer Sci Part A-Polymer Chem* 44(15):4680–4695. doi:[10.1002/pola.21553](https://doi.org/10.1002/pola.21553)
155. Flory PJ (1946) Fundamental principles of condensation polymerization. *Chem Rev* 39(1):137–197. doi:[10.1021/cr60122a003](https://doi.org/10.1021/cr60122a003)
156. Kanazawa H, Ohashi Y, Sasada Y, Kawai T (1982) Polymerization of N-carboxy amino-acid anhydrides in the solid-state. 2. Relation between polymerizability and molecular arrangement in L-leucine NCA and L-alanine NCA crystals. *Journal of Polymer Science Part B-Polymer Physics* 20(10):1847–1862. doi:[10.1002/pol.1982.180201008](https://doi.org/10.1002/pol.1982.180201008)
157. Vayaboury W, Giani O, Cottet H, Deratani A, Schue F (2004) Living polymerization of alpha-amino acid N-carboxyanhydrides (NCA) upon decreasing the reaction temperature. *Macromol Rapid Commun* 25(13):1221–1224. doi:[10.1002/marc.200400111](https://doi.org/10.1002/marc.200400111)
158. Deming TJ (1998) Amino acid derived nickelacycles: intermediates in nickel-mediated polypeptide synthesis. *J Am Chem Soc* 120(17): 4240–4241. doi:[10.1021/ja980313i](https://doi.org/10.1021/ja980313i)
159. Deming TJ (1999) Cobalt and iron initiators for the controlled polymerization of alpha-amino acid-N-carboxyanhydrides. *Macromolecules* 32(13):4500–4502. doi:[10.1021/ma9902899](https://doi.org/10.1021/ma9902899)
160. Deming TJ (2007) Synthetic polypeptides for biomedical applications. *Prog Polym Sci* 32(8–9):858–875. doi:[10.1016/j.progpolymsci.2007.05.010](https://doi.org/10.1016/j.progpolymsci.2007.05.010)
161. Deming TJ (2002) Methodologies for preparation of synthetic block copolypeptides: materials with future promise in drug delivery. *Adv Drug Deliv* 54(8):1145–1155
162. Hadjichristidis N, Iatrou H, Pitsikalis M, Sakellariou G (2009) Synthesis of well-defined polypeptide-based materials via the ring-opening polymerization of alpha-amino acid N-carboxyanhydrides. *Chem Rev* 109(11):5528–5578. doi:[10.1021/cr900049t](https://doi.org/10.1021/cr900049t)
163. Pickel DL, Politakos N, Avgeropoulos A, Messman JM (2009) A mechanistic study of alpha-(amino acid)-N-carboxyanhydride polymerization: comparing initiation and termination events in high-vacuum and traditional polymerization techniques. *Macromolecules* 42(20):7781–7788. doi:[10.1021/ma901340y](https://doi.org/10.1021/ma901340y)
164. Lu H, Cheng JJ (2008) N-trimethylsilyl amines for controlled ring-opening polymerization of amino acid N-carboxyanhydrides and facile end group functionalization of polypeptides. *J Am Chem Soc* 130(38):12562. doi:[10.1021/ja803304x](https://doi.org/10.1021/ja803304x)
165. Yin Q, Tong R, Xu YX, Baek K, Dobrucki LW, Fan TM, Cheng JJ (2013) Drug-initiated ring-opening polymerization of O-carboxyanhydrides for the preparation of anticancer drug-poly(O-carboxyanhydride) nanoconjugates. *Biomacromolecules* 14(3): 920–929. doi:[10.1021/bm301999c](https://doi.org/10.1021/bm301999c)
166. Schlaad, H. (2006) Solution properties of polypeptide-based copolymers. In: Klok HA, Schlaad H (eds). *Peptide hybrid polymers*, 202, pp 53–73
167. Bilek L, Derkusch J, Michl H, Wessely F (1953) *Über die Zersetzung von alpha-amino-n-carbonsaureanhydriden mit Pyridin und Pyridinderivaten - Zur Frage der Bildung von hohermolekularen Cyclopeptiden. *Monatshefte für Chemie* 84(4):717–740. doi:[10.1007/bf00902771](https://doi.org/10.1007/bf00902771)
168. Deming, T. J. (2006) Polypeptide and polypeptide hybrid copolymer synthesis via NCA polymerization. In: Klok HA, Schlaad H (eds) *Peptide hybrid polymers*, 202, pp 1–18
169. Habraken GJM, Heise A, Thornton PD (2012) Block copolypeptides prepared by N-carboxyanhydride ring-opening polymerization. *Macromol Rapid Commun* 33(4):272–286. doi:[10.1002/marc.201100730](https://doi.org/10.1002/marc.201100730)
170. Oya M, Uno K, Iwakura Y (1970) Polymerization of alpha-amino acid N-carboxy anhydride (4-alkyl-oxazolidine-dione). 4. A novel synthesis of a block copolypeptide. *Bull Chem Soc Jpn* 43(6):1788
171. He SJ, Lee C, Gido SP, Yu SJM, Tirrell DA (1998) A twist grain boundary-like twisted smectic phase in monodisperse poly(gamma-benzyl alpha, L-glutamate) produced by recombinant DNA techniques. *Macromolecules* 31(26):9387–9389. doi:[10.1021/ma981286j](https://doi.org/10.1021/ma981286j)
172. Zhang GH, Fournier MJ, Mason TL, Tirrell DA (1992) Biological synthesis of monodisperse derivatives of poly(alpha, L-glutamic acid)—model rodlike polymers. *Macromolecules* 25(13):3601–3603. doi:[10.1021/ma00039a048](https://doi.org/10.1021/ma00039a048)
173. Obeid R, Scholz C (2011) Synthesis and self-assembly of well-defined poly(amino acid) end-capped poly(ethylene glycol) and poly(2-methyl-2-oxazoline). *Biomacromolecules* 12(10):3797–3804. doi:[10.1021/bm201048x](https://doi.org/10.1021/bm201048x)
174. Balik CM, Hopfinger AJ (1978) Quantization of the solvent effect on the adsorption of poly- γ -benzyl-L-glutamate. *J Colloid Interface Sci* 67(1):118–126. doi:[10.1016/0021-9797\(78\)90219-9](https://doi.org/10.1016/0021-9797(78)90219-9)
175. Zheng WW, Frank CW (2010) Surface-Initiated Vapor Deposition Polymerization of Poly(gamma-benzyl-L-glutamate): Optimization and Mechanistic Studies. *Langmuir* 26(6):3929–3941. doi:[10.1021/la9032628](https://doi.org/10.1021/la9032628)
176. Wieringa RH, Siesling EA, Werkman PJ, Vorenkamp EJ, Schouten AJ (2001) Surface grafting of poly(L-glutamates). 3. Block copolymerization. *Langmuir* 17(21):6491–6495. doi:[10.1021/la001771j](https://doi.org/10.1021/la001771j)
177. Ray JG, Johnson AJ, Savin DA (2013) Self-assembly and responsiveness of polypeptide-based block copolymers: how “smart” behavior and topological complexity yield unique assembly in aqueous media. *J Polym Sci, Part B: Polym Phys* 51(7):508–523. doi:[10.1002/polb.23259](https://doi.org/10.1002/polb.23259)
178. Richtering W, Gan D, Lyon LA (2006) Amphiphilic, peptide-modified core/shell microgels. In: *Smart colloidal materials*. Springer, Berlin, pp 1–8
179. Wang XL, Daly WH, Russo P, Ngu-Schwemlein M (2001) Synthesis of paucidisperse poly(gamma-benzyl-alpha, L-glutamate) oligomers and star polymers with rigid arms. *Biomacromolecules* 2(4):1214–1219. doi:[10.1021/bm015569m](https://doi.org/10.1021/bm015569m)
180. Fong B, Turksen S, Russo PS, Stryjewski W (2004) Colloidal crystals of silica-homopolypeptide composite particles. *Langmuir* 20(1):266–269. doi:[10.1021/la034762u](https://doi.org/10.1021/la034762u)
181. Phan SE, Russel WB, Zhu JX, Chaikin PM (1998) Effects of polydispersity on hard sphere crystals. *J Chem Phys* 108(23): 9789–9795. doi:[10.1063/1.476453](https://doi.org/10.1063/1.476453)
182. Kolb HC, Finn MG, Sharpless KB (2001) Click chemistry: diverse chemical function from a few good reactions. *Angew Chem-Int Edit* 40(11):2004. doi:[10.1002/1521-3773\(20010601\)40:11<2004::aidanie2004>3.3.co;2-x](https://doi.org/10.1002/1521-3773(20010601)40:11<2004::aidanie2004>3.3.co;2-x)
183. Golas PL, Matyjaszewski K (2007) Click chemistry and ATRP: a beneficial union for the preparation of functional materials. *QSAR Comb Sci* 26(11–12):1116–1134. doi:[10.1002/qsar.200740059](https://doi.org/10.1002/qsar.200740059)
184. Li NW, Binder WH (2010) Click-chemistry for nanoparticle-modification. *J Mater Chem* 21(42):16717–16734. doi:[10.1039/c1jm11558h](https://doi.org/10.1039/c1jm11558h)
185. Tang HY, Zhang DH (2011) Multi-functionalization of helical block copoly(alpha-peptide)s by orthogonal chemistry. *Polym Chem* 2(7): 1542–1551. doi:[10.1039/c1py00015b](https://doi.org/10.1039/c1py00015b)
186. Agut W, Agnau R, Lecommandoux S, Taton D (2008) Synthesis of block copolypeptides by click chemistry. *Macromol Rapid Commun* 29(12–13):1147–1155. doi:[10.1002/marc.200800123](https://doi.org/10.1002/marc.200800123)

187. Ranjan R, Brittain WJ (2007) Tandem RAFT polymerization and click chemistry: an efficient approach to surface modification. *Macromol Rapid Commun* 28(21):2084–2089. doi:[10.1002/marc.200700428](https://doi.org/10.1002/marc.200700428)
188. Balamurugan SS, Soto-Cantu E, Cueto R, Russo PS (2010) Preparation of organosoluble silica-polypeptide particles by “click” chemistry. *Macromolecules* 43(1):62–70. doi:[10.1021/ma901840n](https://doi.org/10.1021/ma901840n)
189. Kar M, Pauline M, Sharma K, Kumaraswamy G, Sen Gupta S (2011) Synthesis of poly-L-glutamic acid grafted silica nanoparticles and their assembly into macroporous structures. *Langmuir* 27(19):12124–12133. doi:[10.1021/la202036c](https://doi.org/10.1021/la202036c)
190. Kar M, Vijayakumar PS, Prasad BLV, Sen Gupta S (2010) Synthesis and characterization of poly-L-lysine-grafted silica nanoparticles synthesized via NCA polymerization and click chemistry. *Langmuir* 26(8):5772–5781. doi:[10.1021/la903595x](https://doi.org/10.1021/la903595x)
191. Kar M, Tiwari N, Tiwari M, Lahiri M, Sen Gupta S (2013) Poly-L-arginine grafted silica mesoporous nanoparticles for enhanced cellular uptake and their application in DNA delivery and controlled drug release. *Part Part Syst Char* 30(2):166–179. doi:[10.1002/ppsc.201200089](https://doi.org/10.1002/ppsc.201200089)
192. Wittig G, Krebs A (1961) Zur existenz niedergliedriger cycloalkine. I. *Chemische Berichte-Recueil* 94(12):3260–3275. doi:[10.1002/cber.19610941213](https://doi.org/10.1002/cber.19610941213)
193. Himo F, Lovell P, Hilgraf R, Rostovtsev VV, Noddleman L, Sharpless KB, Fokin VV (2005) Copper(I)-catalyzed synthesis of azoles. DFT study predicts unprecedented reactivity and intermediates. *J Am Chem Soc* 127(1):210–216. doi:[10.1021/ja0471525](https://doi.org/10.1021/ja0471525)
194. Jewett JC, Bertozzi CR (2010) Cu-free click cycloaddition reactions in chemical biology. *Chem Soc Rev* 39(4):1272–1279
195. Lin Y-C, Kuo S-W (2012) Hierarchical self-assembly and secondary structures of linear polypeptides graft onto POSS in the side chain through click chemistry. *Polym Chem* 3(1):162–171
196. Wieringa RH, Siesling EA, Geurts PFM, Werkman PJ, Vorenkamp EJ, Erb V, Stamm M, Schouten AJ (2001) Surface grafting of poly(L-glutamates). I. Synthesis and characterization. *Langmuir* 17(21):6477–6484. doi:[10.1021/la001769s](https://doi.org/10.1021/la001769s)
197. Luijten J, Groeneveld DY, Nijboer GW, Vorenkamp EJ, Schouten AJ (2007) Cross-linking-induced permanently perpendicular helix orientation in surface-grafted polyglutamate films. *Langmuir* 23(15):8163–8169. doi:[10.1021/la07005106](https://doi.org/10.1021/la07005106)
198. Wieringa RH, Schouten AJ (1996) Oriented thin film formation by surface graft polymerization of gamma-methyl L-glutamate N-carboxyanhydride in the melt. *Macromolecules* 29(8):3032–3034. doi:[10.1021/ma9508358](https://doi.org/10.1021/ma9508358)
199. Chang, Y. C.; Frank, C. W. (1998) Chemical grafting of poly(L-glutamate) gamma-esters on silicon (100) surfaces by vapor polymerization of N-carboxy anhydride monomers. In: Frank CW (ed) Organic thin films: structure and applications, 695, pp 142–157
200. Soto-Cantu E, Turksen-Selcuk S, Qiu JH, Zhou Z, Russo PS, Henk MC (2011) Silica-polypeptide composite particles: controlling shell growth. *Langmuir* 26(19):15604–15613. doi:[10.1021/la1023955](https://doi.org/10.1021/la1023955)
201. Wyatt PJ (1970) Cell wall thickness, size distribution, refractive index ratio and dry weight content of living bacteria (*Staphylococcus aureus*). *Nature* 226(5242):277. doi:[10.1038/226277a0](https://doi.org/10.1038/226277a0)
202. Bu MQ, Melvin T, Ensell GJ, Wilkinson JS, Evans AGR (2004) A new masking technology for deep glass etching and its microfluidic application. *Sensor Actuat A-Phys* 115(2–3):476–482. doi:[10.1016/j.sna.2003.12.013](https://doi.org/10.1016/j.sna.2003.12.013)
203. Fasman GD, Idelson M, Blout ER (1961) Synthesis and conformation of high molecular weight poly-epsilon-carbobenzoyloxy-L-lysine and poly-L-lysine.HCl. *J Am Chem Soc* 83(3):709
204. Liu D, Li Y, Deng JP, Yang WT (2011) Synthesis and characterization of magnetic Fe_3O_4 -silica-poly(gamma-benzyl-L-glutamate) composite microspheres. *React Funct Polym* 71(10):1040–1044. doi:[10.1016/j.reactfunctpolym.2011.07.009](https://doi.org/10.1016/j.reactfunctpolym.2011.07.009)
205. Ostlund SG, Striegel AM (2008) Ultrasonic degradation of poly(gamma-benzyl-L-glutamate), an archetypal highly extended polymer. *Polym Degrad Stabil* 93(8):1510–1514. doi:[10.1016/j.polymdegradstab.2008.05.012](https://doi.org/10.1016/j.polymdegradstab.2008.05.012)
206. Xu Z, Feng Y, Liu X, Guan M, Zhao C, Zhang H (2010) Synthesis and characterization of $\text{Fe}_3\text{O}_4@SiO_2@poly\text{-}l\text{-alanine}$, peptide brush magnetic microspheres through NCA chemistry for drug delivery and enrichment of BSA. *Colloids Surf B* 81(2):503–507. doi:[10.1016/j.colsurfb.2010.07.048](https://doi.org/10.1016/j.colsurfb.2010.07.048)
207. Johnston APR, Cortez C, Angelatos AS, Caruso F (2006) Layer-by-layer engineered capsules and their applications. *Curr Opin Colloid Interface Sci* 11(4):203–209. doi:[10.1016/j.cocis.2006.05.001](https://doi.org/10.1016/j.cocis.2006.05.001)
208. Becker AL, Johnston APR, Caruso F (2010) Layer-by-layer-assembled capsules and films for therapeutic delivery. *Small* 6(17):1836–1852. doi:[10.1002/smll.201000379](https://doi.org/10.1002/smll.201000379)
209. Wiedeman MP (1963) Dimensions of blood vessels from distributing artery to collecting vein. *Circ Res* 12(4):375
210. Zelikin AN, Li Q, Caruso F (2008) Disulfide-stabilized poly(methacrylic acid) capsules: formation, cross-linking, and degradation behavior. *Chem Mat* 20(8):2655–2661. doi:[10.1021/cm703403p](https://doi.org/10.1021/cm703403p)
211. Johnston APR, Zelikin AN, Caruso F (2007) Assembling DNA into advanced materials: from nanostructured films to biosensing and delivery systems. *Adv Mater* 19(21):3727–3730. doi:[10.1002/adma.200701147](https://doi.org/10.1002/adma.200701147)
212. Yan Y, Ochs CJ, Such GK, Heath JK, Nice EC, Caruso F (2010) Bypassing multidrug resistance in cancer cells with biodegradable polymer capsules. *Adv Mater* 22(47):5398. doi:[10.1002/adma.201003162](https://doi.org/10.1002/adma.201003162)
213. Hosta-Rigau L, Stadler B, Yan Y, Nice EC, Heath JK, Albericio F, Caruso F (2010) Capsosomes with multilayered subcompartments: assembly and loading with hydrophobic cargo. *Adv Funct Mater* 20(1):59–66. doi:[10.1002/adfm.200901297](https://doi.org/10.1002/adfm.200901297)
214. Chandrawati R, van Koeverden MP, Lomas H, Caruso F (2011) Multicompartment particle assemblies for bioinspired encapsulated reactions. *J Phys Chem Lett* 2(20):2639–2649. doi:[10.1021/jz200994n](https://doi.org/10.1021/jz200994n)
215. Chang DHC, Johnston APR, Wark KL, Breheney K, Caruso F (2012) Engineered bacterially expressed polypeptides: assembly into polymer particles with tailored degradation profiles. *Angew Chem-Int Edit* 51(2):460–464. doi:[10.1002/anie.201106033](https://doi.org/10.1002/anie.201106033)
216. Peabody DS, Manifold-Wheeler B, Medford A, Jordan SK, do Carmo Caldeira J, Chackerian B (2008) Immunogenic display of diverse peptides on virus-like particles of RNA phage MS2. *J Mol Biol* 380(1):252–263
217. McPherson A (2005) Micelle formation and crystallization as paradigms for virus assembly. *Bioessays* 27(4):447–458. doi:[10.1002/bies.20196](https://doi.org/10.1002/bies.20196)
218. Marcelo G, Munoz-Bonilla A, Fernandez-Garcia M (2012) Magnetite-polypeptide hybrid materials decorated with gold nanoparticles: study of their catalytic activity in 4-nitrophenol reduction. *J Phys Chem C* 116(46):24717–24725. doi:[10.1021/jp309145r](https://doi.org/10.1021/jp309145r)
219. Marcelo G, Munoz-Bonilla A, Rodriguez-Hernandez J, Fernandez-Garcia M (2013) Hybrid materials achieved by polypeptide grafted magnetite nanoparticles through a dopamine biomimetic surface anchored initiator. *Polym Chem* 4(3):558–567. doi:[10.1039/c2py20514a](https://doi.org/10.1039/c2py20514a)
220. Borase T, Ninjabdar T, Kapetanakis A, Roche S, O'Connor R, Kerskens C, Heise A, Brougham DF (2013) Stable aqueous dispersions of glycopeptide-grafted selectively functionalized magnetic nanoparticles. *Angew Chem Int Edit* 52(11):3164–3167. doi:[10.1002/anie.201208099](https://doi.org/10.1002/anie.201208099)
221. Maccarrone S, Brambilla G, Pravaz O, Duri A, Ciccotti M, Fromental JM, Pashkovski E, Lips A, Sessoms D, Trappe V, Cipelletti L (2010) Ultra-long range correlations of the dynamics

- of jammed soft matter. *Soft Matter* 6(21):5514–5522. doi:[10.1039/c0sm00155d](https://doi.org/10.1039/c0sm00155d)
222. Coniglio A, Abete T, de Candia A, Del Gado E, Fierro A (2008) Dynamical heterogeneities: from glasses to gels. *J. Phys.: Condens. Matter*, 20:494239
223. Siebenburger M, Fuchs M, Ballauff M (2012) Core–shell microgels as model colloids for rheological studies. *Soft Matter* 8(15):4014–4024. doi:[10.1039/c2sm07011a](https://doi.org/10.1039/c2sm07011a)
224. Lhuillier D, Nadim A (2010) Rheology of suspensions of mass-polarized particles in a gravitational field. *Chem Eng Commun* 197(1):76–91. doi:[10.1080/00986440903070742](https://doi.org/10.1080/00986440903070742)
225. de Folter JWJ, de Villeneuve VWA, Aarts D, Lekkerkerker HNW (2010) Rigid sphere transport through a colloidal gas–liquid interface. *New J. Phys.*, 12:023013
226. Finsy R, Moreels E, Bottger A, Lekkerkerker H (1985) Study of the relation between diffusion and sedimentation of charged silica sols by dynamic light-scattering, ultracentrifugation, and turbidimetry. *J Chem Phys* 82(8):3812–3816
227. Almenar L, Rauscher M (2011) Dynamics of colloids in confined geometries. *J Phys Condens Matter* 23(18):184115
228. Tracy MA, Garcia JL, Pecora R (1993) An investigation of the microstructure of a rod sphere composite liquid. *Macromolecules* 26(8):1862–1868. doi:[10.1021/ma00060a011](https://doi.org/10.1021/ma00060a011)
229. Pawsey AC, Lintuvuori JS, Wood TA, Thijssen JHJ, Marenduzzo D, Clegg PS (2012) Colloidal particles at the interface between an isotropic liquid and a chiral liquid crystal. *Soft Matter* 8(32):8422–8428. doi:[10.1039/c2sm25434d](https://doi.org/10.1039/c2sm25434d)
230. Svoboda K, Block SM (1994) Biological applications of optical forces. *Annu Rev Biophys Biomol Struct* 23:247–285. doi:[10.1146/annurev.bb.23.060194.001335](https://doi.org/10.1146/annurev.bb.23.060194.001335)
231. Gutsche C, ElMahdy MM, Kegler K, Semenov I, Stangner T, Otto O, Ueberschar O, Keyser UF, Krueger M, Rauscher M, Weeber R, Harting J, Kim YW, Lobaskin V, Netz RR, Kremer F (2011) Micro-rheology on (polymer-grafted) colloids using optical tweezers. *J. Phys.: Condens. Matter*, 23:184114
232. Castelain M, Rouxhet PG, Pignon F, Magnin A, Piau JM (2012) Single-cell adhesion probed in-situ using optical tweezers: a case study with *Saccharomyces cerevisiae*. *J. Appl. Phys.*, 111(11)
233. Hegge S, Uhrig K, Streichfuss M, Kynast-Wolf G, Matuschewski K, Spatz JP, Frischknecht F (2012) Direct manipulation of malaria parasites with optical tweezers reveals distinct functions of plasmodium surface proteins. *ACS Nano* 6(6):4648–4662. doi:[10.1021/nn203616u](https://doi.org/10.1021/nn203616u)
234. Sanson C, Le Meins JF, Schatz C, Soum A, Lecommandoux S (2010) Temperature responsive poly(trimethylene carbonate)-block-poly(L-glutamic acid) copolymer: polymersomes fusion and fission. *Soft Matter* 6(8):1722–1730. doi:[10.1039/b924617g](https://doi.org/10.1039/b924617g)
235. Sanson C, Schatz C, Le Meins JF, Brulet A, Soum A, Lecommandoux S (2010) Biocompatible and biodegradable poly(trimethylene carbonate)-b-poly (L-glutamic acid) polymersomes: size control and stability. *Langmuir* 26(4):2751–2760. doi:[10.1021/la902786t](https://doi.org/10.1021/la902786t)
236. Sanson C, Diou O, Thevenot J, Ibarboure E, Soum A, Brulet A, Miraux S, Thiaudiere E, Tan S, Brisson A, Dupuis V, Sandre O, Lecommandoux S (2011) Doxorubicin loaded magnetic polymersomes: theranostic nanocarriers for MR imaging and magneto-chemotherapy. *ACS Nano* 5(2):1122–1140. doi:[10.1021/nn102762f](https://doi.org/10.1021/nn102762f)
237. Huang J, Bonduelle C, Thevenot J, Lecommandoux S, Heise A (2012) Biologically active polymersomes from amphiphilic glycopeptides. *J Am Chem Soc* 134(1):119–122. doi:[10.1021/ja209676p](https://doi.org/10.1021/ja209676p)
238. Lau KHA, Duran H, Knoll W (2009) In situ characterization of N-carboxy anhydride polymerization in nanoporous anodic alumina. *J Phys Chem B* 113(10):3179–3189. doi:[10.1021/jp809593d](https://doi.org/10.1021/jp809593d)
239. Chandrawati R, Hosta-Rigau L, Vanderstraeten D, Lokuliyana SA, Stadler B, Albericio F, Caruso F (2010) Engineering advanced capsosomes: maximizing the number of subcompartments, cargo retention, and temperature-triggered reaction. *ACS Nano* 4(3):1351–1361. doi:[10.1021/nn901843j](https://doi.org/10.1021/nn901843j)